Cell Reports

Article

Human FACT subunits coordinate to catalyze both disassembly and reassembly of nucleosomes

Graphical abstract

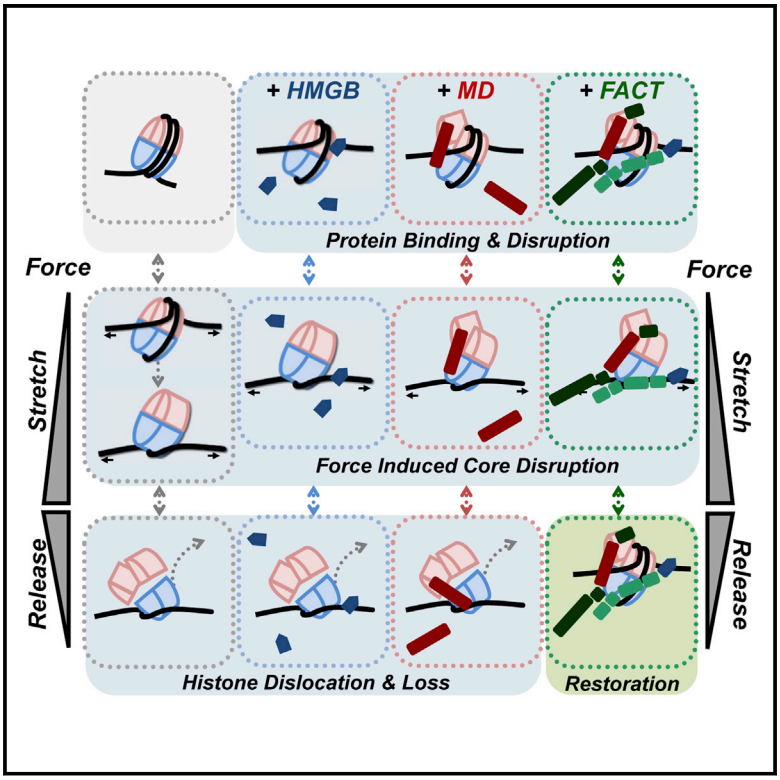

Authors

Micah J. McCauley, Michael Morse, Nicole Becker, ..., Georges Mer, L. James Maher III, Mark C. Williams

Correspondence

ma.williams@northeastern.edu

In brief

McCauley et al. use single-molecule methods to determine the stability and dynamics of nucleosomes with the histone chaperone FACT. Two FACT domains exhibit activity: SSRP1 HMGB domain displaces DNA, while SPT16 MD/CTD stabilizes DNA-H2A/H2B interactions. However, only intact FACT tethers disrupted DNA to histones, supporting rapid nucleosome reassembly.

Highlights

- FACT binding destabilizes DNA-histone interactions, leading to partial DNA loss
- SSRP1 HMGB displaces DNA, while SPT16 MD/CTD stabilizes DNA-H2A/H2B interactions
- Only the full FACT protein catalyzes both nucleosome disassembly and reassembly

McCauley et al., 2022, Cell Reports *41*, 111858
December 27, 2022
https://doi.org/10.1016/j.celrep.2022.111858

CellPress

Cell Reports

CellPress
OPEN ACCESS

Article

Human FACT subunits coordinate to catalyze both disassembly and reassembly of nucleosomes

Micah J. McCauley,[1] Michael Morse,[1] Nicole Becker,[2] Qi Hu,[2] Maria Victoria Botuyan,[2] Emily Navarrete,[1] Ran Huo,[1] Uma M. Muthurajan,[3] Ioulia Rouzina,[4] Karolin Luger,[3,5] Georges Mer,[2] L. James Maher III,[2] and Mark C. Williams[1,6,*]

[1]Department of Physics, Northeastern University, Boston, MA, USA
[2]Department of Biochemistry and Molecular Biology, Mayo Clinic College of Medicine and Science, Rochester, MN, USA
[3]Department of Biochemistry, University of Colorado, Boulder, CO, USA
[4]Department of Chemistry and Biochemistry, Ohio State University, Columbus, OH 43210, USA
[5]Howard Hughes Medical Institute, Chevy Chase, MD 20815, USA
[6]Lead contact
*Correspondence: ma.williams@northeastern.edu
https://doi.org/10.1016/j.celrep.2022.111858

SUMMARY

The histone chaperone FACT (facilitates chromatin transcription) enhances transcription in eukaryotic cells, targeting DNA-protein interactions. FACT, a heterodimer in humans, comprises SPT16 and SSRP1 subunits. We measure nucleosome stability and dynamics in the presence of FACT and critical component domains. Optical tweezers quantify FACT/subdomain binding to nucleosomes, displacing the outer wrap of DNA, disrupting direct DNA-histone (core site) interactions, altering the energy landscape of unwrapping, and increasing the kinetics of DNA-histone disruption. Atomic force microscopy reveals nucleosome remodeling, while single-molecule fluorescence quantifies kinetics of histone loss for disrupted nucleosomes, a process accelerated by FACT. Furthermore, two isolated domains exhibit contradictory functions; while the SSRP1 HMGB domain displaces DNA, SPT16 MD/CTD stabilizes DNA-H2A/H2B dimer interactions. However, only intact FACT tethers disrupted DNA to the histones and supports rapid nucleosome reformation over several cycles of force disruption/release. These results demonstrate that key FACT domains combine to catalyze both nucleosome disassembly and reassembly.

INTRODUCTION

The nucleosome is the basic subunit of chromatin, which compacts, organizes, and protects DNA from damage. The nucleosome is composed of 147 base pairs (bp) of DNA, wrapped ~1.7 times around a protein core consisting of four pairs of histones: H2A, H2B, H3, and H4 (Figure 1A).[1] Both H3-H4 pairs dimerize at the H3 α3 helix to form the tetramer (Figure 1B), while two dimers of H2A/H2B complete the symmetric structure of the octamer (Figure 1C). DNA is wrapped around the octamer up to ±40 bp from the axis, bent to both the $(H3\text{-}H4)_2$ tetramer and the H2A/H2B dimers. This inner core of wrapped DNA is held at these critical "strong sites" where the charged DNA backbone meets the $(H3\text{-}H4)_2$ tetramer and the H2A/H2B dimers.[2,3] Two outer half wraps of DNA, ±35 bp beyond the core, are more weakly coordinated to the octamer (Figure 1D). DNA is anchored by direct DNA-histone contacts with the H2A/H2B dimers and $(H3\text{-}H4)_2$ tetramer as well as with long unstructured histone tails. Finally, linker DNA (60 bp as shown in Figure 1D) separates adjacent nucleosomes.

FACT (facilitates chromatin transcription) is a conserved histone chaperone that can both destabilize and reassemble nucleosomes (Figure 1E).[8–14] FACT is a heterodimer containing SPT16 paired with either Pob3 (in fungi) or SSRP1 (in higher eukaryotes), where each subunit comprises multiple histone-binding modules connected by unstructured linkers.[4,5,11,15,16] A recent cryo-EM structure of FACT bound to a hexamer (Figure 1F) revealed domains binding in a "saddle" conformation, as dimerized DD domains contact the DNA attached to the dyad site while connecting the FACT "legs."[6] SSRP1 and SPT16 each contain MD subdomains contacting individual histones, as well as the inner wrap DNA on the opposite sides of the core, while the SPT16 CTD domain serves the critical function of binding to and helping to tether H2A/H2B dimers as DNA is displaced (the SSRP1 CTD is not shown).[6,16] Another key functional DNA-binding domain (not present in Figure 1F), high mobility group B (HMGB), is known to bind and displace DNA from the nucleosome (Figure 1G).[17,18] HMGB family member Nhp6A provides this function in yeast.[17,19,20] Thus, full FACT uses these domains to bind multiple sites on nucleosomes, sequentially exposing and engaging additional buried sites to produce an altered "reorganized" nucleosome.[8,11,15,17,21] The nucleosome reassembly activity of FACT is then proposed to catalyze reversal of these steps.[22] However, it is not understood how the structural elements of this large heterodimeric protein coordinate to both destabilize nucleosomes yet also facilitate the seemingly opposite process of reassembly.

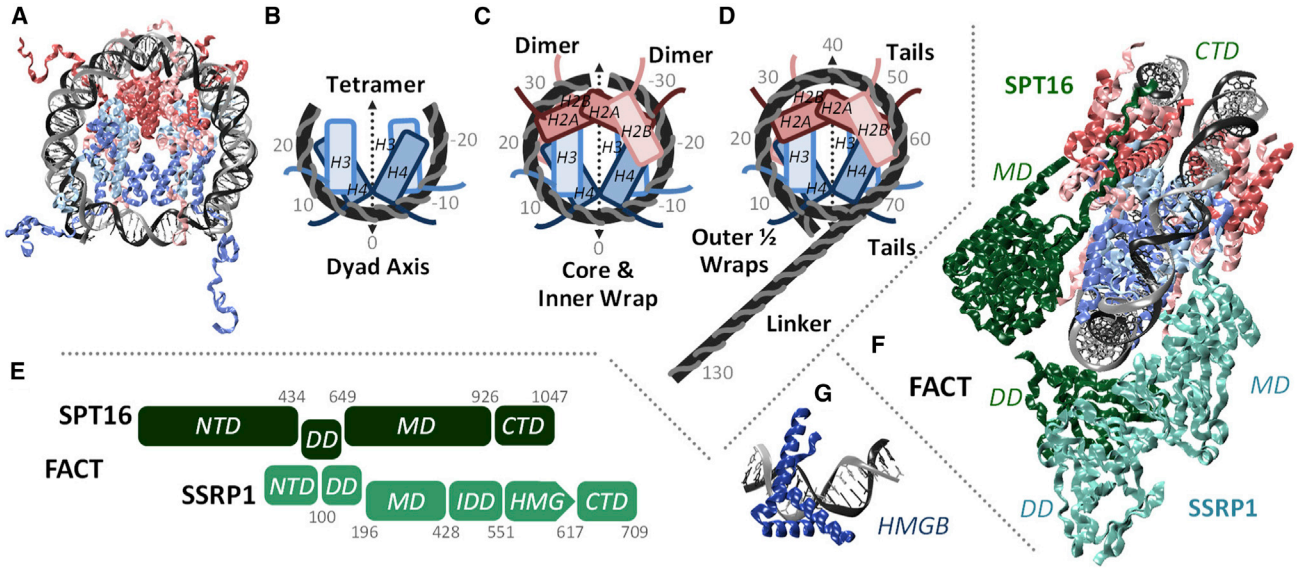

Figure 1. Probing histone-DNA interactions under the influence of FACT

(A–D) (A) The complete nucleosome (PDB: 1kx5)[3] consists of DNA (gray/silver) wrapped around (B) the central dyad of the $(H3\text{-}H4)_2$ tetramer (cyan/blue) and (C) a pair of H2A/H2B dimers (red/pink). DNA is held to these core "strong sites" while (D) the outer two half wraps of DNA are more weakly organized by contacts with histone coils and tails.

(E) Heterodimeric full hFACT is composed of subunits SPT16 (forest) and SSRP1 (green), with subdomains, including NTD (N-terminal domain), DD (dimer domain), MD (middle domain), IDD (intrinsically disordered domain), CTD (C-terminal domain), and HMGB (high mobility group B).[4,5]

(F) The SPT16 subunit binds to and dislocates the DNA-H2A/H2B dimer-DNA interactions in this hexamer (PDB: 6upl).[6] Only the inner DNA wrap is imaged here and the SSRP1 HMGB domain is not present. Color coding matches previous panels.

(G) The HMGB domain (blue) binds to and bends bare DNA (silver) (PDB: 1ckt).[7]

Cellular FACT concentrations vary widely in different tissues and stages of differentiation.[20,23–27] Moreover, FACT appears to function selectively based on genomic location, cell type, and circumstance. FACT is significantly enriched at coding regions of highly transcribed genes.[28] FACT expression is also significantly higher in both human and mouse tumor cell lines[29,30] and tumors.[23,31] Elevated FACT expression is observed in cells expressing cancer stem cell markers.[32–34] Furthermore, cells with high FACT expression are more vulnerable to killing by FACT depletion.[34] These observations suggest that tumor cells require higher concentrations of FACT, suggesting a rationale for FACT inhibition as a therapeutic approach.[35]

FACT strongly facilitates transcription *in vitro*,[5,9,36–39] although its importance for high transcription rates *in vivo* has been questioned.[35,40] However, there is clear evidence that chromatin is destabilized by RNA polymerase (RNAP), and FACT influences chromatin structure,[8,41] perhaps by depositing histone dimers onto histone hexamers.[12,22] As free histones are highly toxic to yeast[42] and mammalian cells (Gurova et al.[13]), it is possible that FACT protects cells executing chromatin transactions that generate free histones (transcription, replication, DNA repair). In contrast, cells less engaged in these transactions may not accumulate free histones to toxic levels even upon FACT depletion. It has thus been suggested that the primary role of FACT is to prevent accumulation of these free histones shed during chromatin transactions.[43] The ability of FACT to facilitate nucleosome reassembly suggests a role in preventing histone variants from becoming histone "deviants."[44]

In this work, we employ single-molecule force disruption and survival probability experiments with optical tweezers (OT), as well as AFM and single-molecule fluorescence (SMF) imaging. We characterize the activity of the full FACT complex and identify key isolated subdomains; SSRP1 HMGB and SPT16 MD. We show that FACT binding destabilizes the nucleosome, releasing DNA from the outer half wraps, increasing DNA-histone fluctuations throughout the nucleosome and reducing the total energy of DNA-histone interactions by almost half. Within FACT, the SSRP1 HMGB domain binds directly to bent DNA near the entry of the nucleosome, weakening DNA-histone contacts throughout. In contrast, SPT16 MD weakly stabilizes the strong site-DNA interactions within the nucleosome, likely by binding to DNA and the H2A/H2B dimer. While disrupted nucleosomes remain associated with the DNA at the dyad axis, intact FACT, SSRP1 HMGB, and SPT16 MD all facilitate rapid octamer dissociation. Yet only the combined effects of the two key domains plus the tethering ability of the SPT16 CTD domain in the full FACT complex facilitates nucleosome restoration upon the release of tension. Thus, FACT acts as a true catalyst, lowering the energy barrier to nucleosome reorganization.

RESULTS

Measuring histone-DNA interactions during nucleosome disruption

A typical force-extension curve for an array of nucleosomes formed at Widom 601 sequences (Figure 2A) is shown in

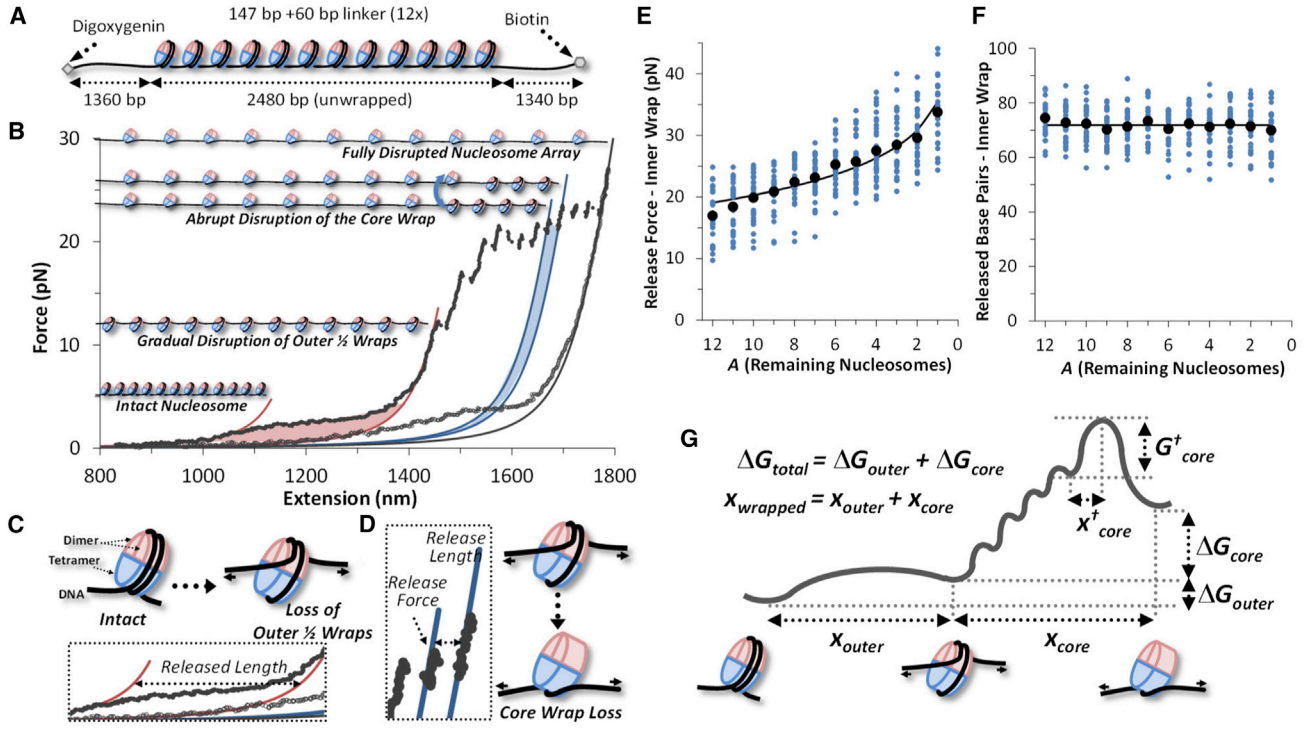

Figure 2. Quantifying nucleosome stability

(A) The probes used in this study consist of a series of 12 × 207-bp Widom 601 positioning sequences flanked by two tagged handles, each labeled by digoxygenin/biotin (shown) or biotin/biotin tags for bead attachment.

(B) Cycles of array extension/release disrupt nucleosomes in distinct stages that are only partially reversible upon release. Polymer models (solid lines, Equation 1) bracket outer wrap release (red), a single inner wrap disruption (blue), and the final full DNA (black). Averaged values of the disruption force and wrapped lengths are shown in Table S1. Shaded regions denote work done during unwrapping. Release partially restores wrapping.

(C and D) Close-ups of release show that forced release of the outer half wraps of DNA from the nucleosome occurs smoothly and indistinctly at low force, whereas DNA-core (strong site) disruptions of the inner wrap are seen as individual high force "rips."

(E) Core release force increases with order of release (*A* for n = 30 arrays, blue) and this variation is fit to a kinetic model of Equation 2 (solid line to averages in black circles, with SEM smaller than the symbols used).

(F) DNA inner wrap length held by each octamer does not change with the order of release (individual measurements in blue are averaged in black, with SEM smaller than the symbols used).

(G) Modeled free energy landscape, identifying the key energies and lengths measured in this work and summarized in Table S2.

Figure 2B, where increasing extension causes increased tension across the overall construct due to the elasticity of the flanking DNA handle and the linker DNA separating sequential nucleosomes.[45–50] This force response is well known and is modeled for varying lengths of DNA (see STAR Methods and Figure S1).[2,12,18] Increasing tension not only destabilizes histone-DNA interactions but also drives the release of free double-stranded DNA (dsDNA) as histone-DNA contacts are disrupted.[2,18] The shortest contour length corresponds to fully wrapped nucleosomes and the longest to the full length of the free duplex DNA construct. Between these two extremes, the measured length of the construct increases in two distinct phases. At forces below 10 pN, the two outer half wraps of DNA are smoothly released from each nucleosome in equilibrium. Higher forces (typically above 10 pN) reveal "rips," corresponding to the individual non-equilibrium peeling of DNA from the core that bind the inner 75 bp of dsDNA to the octamer, leaving only direct DNA contacts with the central dyad (these cannot be readily disrupted by increased DNA tension).[2,12,18]

Although individual release events involving the outer half wraps of DNA are not resolved (Figure 2C), release of the core DNA can be characterized by the measured force and released DNA length (Figure 2D). These measured values may be plotted for the observed order of array disruption. Values observed for analysis of n = 30 arrays and averaged results are shown for release length in Figures 2E and 2F (see also Figure S2). As the lengths are converted to base pairs of DNA, the measured outer and inner wrap release may be summed to give the total DNA wrapped into nucleosomes ($x_{wrapped}$). Although the length released does not vary across the array (Figure 2F), the measured force during inner wrap release increases as the number of remaining nucleosomes (*A*) decreases (Figure 2E). This effect results from the higher pulling rate (nm/s/nucleosome) as fewer octamers remain on DNA, with higher pulling rates leading to increased ripping forces. Thus, the 12-nucleosome array studied here facilitates the study of the force-dependent opening rate ($k(F)$, see also Figure S2). Fitting this model to the averaged release data from n = 30 arrays gives a natural rate of histone-DNA

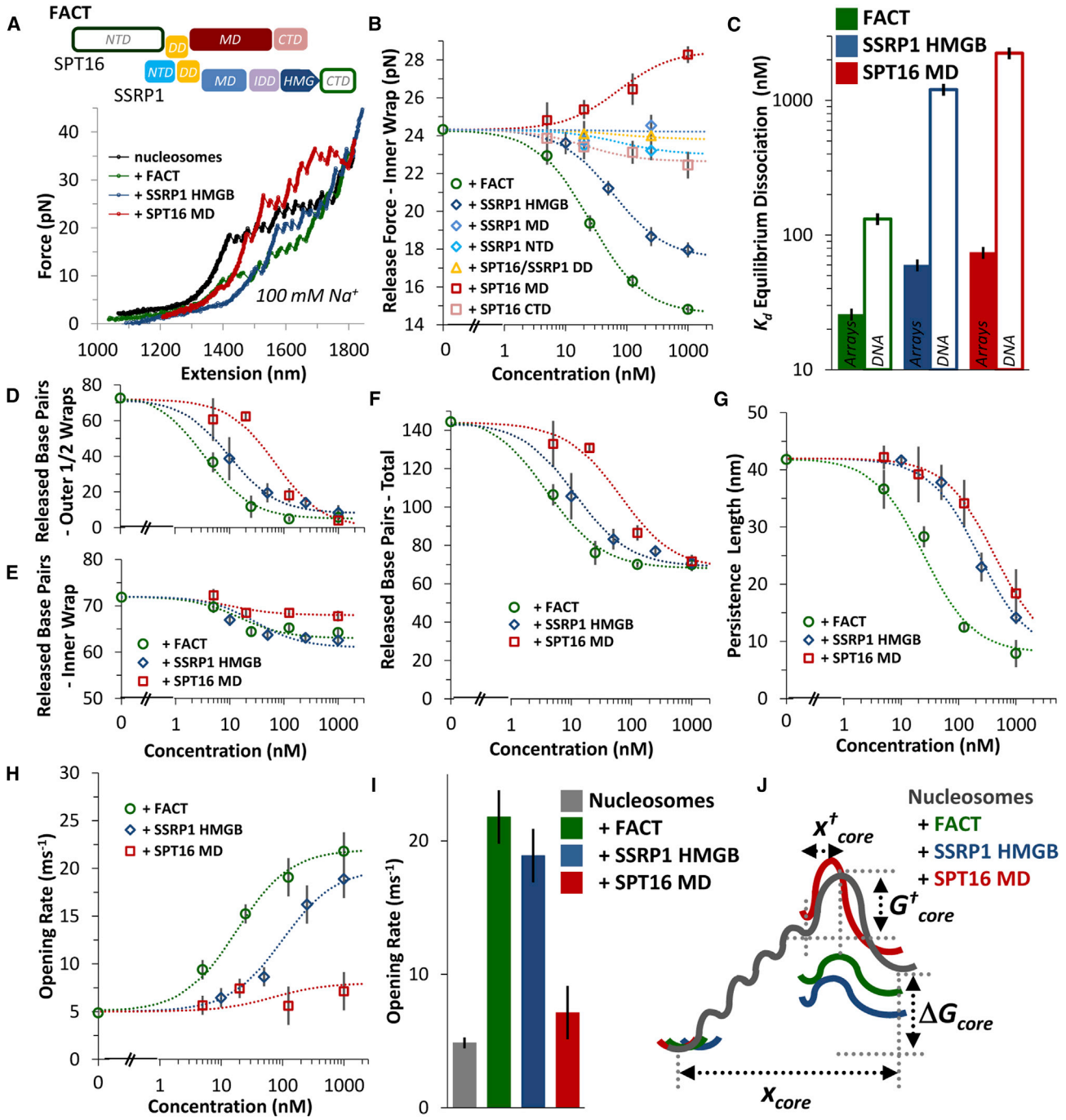

Figure 3. Quantifying activity of FACT and 2 key subdomains

(A) Upper: color key of the FACT protein subunits characterized in the following panels. Lower: force extension curves of the first cycle of extension/release for an array (black), and an array with saturating concentrations of full FACT (green), and subdomains SSRP1 HMGB (blue) and SPT16 MD (red).

(B) Averaged core (inner wrap) release force decreases with increasing FACT concentration (green) and with isolated subunit SSRP1 HMGB concentration (blue) and increases with increasing amounts of the SPT16 MD (red). There is no change within uncertainty for isolated SSRP1 MD (light blue), SSRP1 NTD (cyan), SSRP1/Sprt16 DD (gold), or the SPT16 CTD (pink) domains studied here ($n \geq 5$ arrays for active proteins, with SEM, for n = 163 arrays and N = 1,875 total release events). Dotted lines are fits to a binding isotherm (Equations 3 and 4) for domains that are independently active (and are guides otherwise).

(C–F) (C) Fitted values of equilibrium binding energy (K_D) from (B) (solid bars) are shown for full FACT (green), HMGB (blue), and MD (red). DNA length held by the octamer (and released by external force during extension) decreases in the presence of FACT, SSRP1 HMGB, and SPT16 MD subdomains for (D) the outer half wraps, (E) the inner core wrap, and (F) the total length of DNA bound to the nucleosome. Errors are SEM for $n \geq 5$ arrays.

(legend continued on next page)

fluctuations for this last step in strong site disruption of $k_o = (4.9 \pm 0.4) \times 10^{-3}$ s^{-1}, in reasonable agreement with previous results with *Xenopus* octamers (where $k_o = (3.1 \pm 0.4) \times 10^{-3}$ s^{-1}).[18] Averaged across all *A* and n, values of the release force (F_{avg}) and the wrapped length ($x_{wrapped}$) appear in Table S1.

Scrutinizing the force-extension data gives insight into the energy landscape of force disruption, as illustrated in Figure 2G. The free energy of unwrapping is determined from the total (integrated) energy required to extend the wrapped state less the energy required to extend the unwrapped state to the same release force.[51,52] This is done for both the indistinguishable 12 outer half wrap releases up to ~5 pN and the individually observed rips corresponding to release from the strong sites. Crucially, while the former is an equilibrium process, the latter is not, requiring non-equilibrium techniques to extract the equilibrium free energy (see Figure S3 for details).[53] The energy required to disrupt the outer half wraps was found to be $\Delta G_{outer} = 14 \pm 2$ k_BT. The energy characterizing strong site interactions of the core was higher; $\Delta G_{core} = 62 \pm 4$ k_BT. These values are in reasonable agreement with a previous estimate on isolated nucleosomes.[2] The barrier height to inner wrap release may also be estimated from the distributions of the force release averaged over each value of *A*, to give $G^{\dagger}_{core} = 22 \pm 7$ k_BT (see Figure S4 for details). The free energy of the transition barrier ($G^{\dagger}_{core}$) and the distance to the barrier ($x^{\dagger}_{core}$) for the strong site release appear to be much smaller than the total stability and the DNA length associated with the release of the strong site. Thus, the strong site is released through several smaller substates and the strongest interaction occurs at the last few DNA base pairs bound to the strong site, in agreement with high-resolution maps of nucleosome unwinding.[54] All energy landscape results and the natural rate of opening (including k_o and $x^{\dagger}_{core}$ found above) are found in Table S2 and summarized graphically in Figure 2G.

Roles of FACT SSRP1 HMGB and SPT16 MD domains in nucleosome destabilization

Force disruption of isolated nucleosome arrays was repeated in the presence of increasing concentrations of full FACT (minus the NTD domain of SPT16, and the CTD domain of SSRP1, as discussed in STAR Methods) or various isolated FACT domains (Figure 3A). Measured disruptions of the inner DNA wrap around the octamer core (Figure 3B) allow us to quantify the strength and affinity of DNA-histone interactions in the presence of full FACT (green) and of several isolated domains (color key in Figure 3A). While the HMGB domain (blue) *destabilizes* DNA-histone interactions, consistent with the behavior of full FACT and in agreement with previous work,[11,18] the SPT16 MD (red) *stabilizes* the strong site interactions. Plotting the averaged array release force with increasing concentration reveals binding up to saturation. Dotted lines (Figure 3B) are fits to a binding isotherm, yielding equilibrium dissociation constants (K_D) for direct binding to the nucleosome, summarized in Figure 3C and Table S1. Interestingly these affinities are notably weaker than those observed earlier for isolated Nhp6A and HMO1 ($K_D \sim$ 10–100 nM here compared with 0.1–1 nM earlier).[18] No statistically significant changes in nucleosome stability were induced by the other isolated domains studied here (SSRP1 MD, SSRP1 NTD, SSRP1/SPT16, SPT16 CTD) at concentrations up to 1 μM (the dotted lines here are not fits, but guides to the eye). Interestingly, only a modest effect was seen for SPT16 CTD, which is known to bind to the H2A/H2B dimer.[6,16] However, the isolated CTD domain used here is disorganized and is likely less effective when not coordinated by the neighboring MD domain (for the full protein, other subunits may also have contributions to nucleosome binding). The likely role of SPT16 CTD within full FACT is discussed below. Subsequent data therefore highlight full FACT and the active isolated domains SPT16 MD and SSRP1 HMGB.

The lengths of DNA released during core disruption, occurring in distinct steps for the outer half wraps and the inner wrap (Figures 3D and 3E and summed in 3F) are shown for full FACT vs. the two active domains. Addition of full FACT or individual domains lead to the dissociation of the outer half wraps of DNA from the octamer up to the strong sites (Figure 3D), while the inner DNA wrap is only slightly released from the inner core (Figure 3E). To test affinity for dsDNA, FACT and its active domains were exposed to bare dsDNA constructs. Binding of these proteins to bare DNA is discerned by changes in the persistence length (P_{ds}) fit to the force-extension data (Figure S1).[49,55] Fitting the change in P_{ds} to a simple binding isotherm also measures the equilibrium dissociation constant ($K_{d\ DNA}$). Notably, the fitted persistence length decreases for FACT and the active subunit SSRP1 HMGB, although with reduced affinity compared with that for the complete nucleosome. This feature has been observed before and is attributed to the known preference of HMGB for DNA deformed in the nucleosome.[7,18,49,56] DNA binding by SPT16 MD is much weaker and its effect on DNA persistence length is minimal (Figure 3G). Measured dsDNA and nucleosome affinities are compared in Figure 3C and summarized in Table S1.

Fits of the averaged release force to the kinetic model (Equation 2) reveal that full FACT and SSRP1 HMGB increase nucleosome breathing (Figure 3H), indicating weaker contacts with DNA along the strong sites at the octamer core. Fitted values of the maximum opening rate ($k_o(saturated)$) are shown in Figure 3I. In the presence of saturating concentrations of FACT, HMGB and MD both the release energies for the outer half wraps and the core were measured. Under these conditions, the outer half wraps free energy change was found to disappear; $\Delta G_{outer} \sim 0$ k_BT, consistent with the complete release of outer wrap DNA (above). The

(G) Protein binding to bare dsDNA induces measurable change in the persistence length plotted against concentration. Fitted binding affinity for dsDNA (Equation 5) is weaker than that for nucleosome arrays by an order of magnitude for each subunit and summarized in (C). Errors are SEM for n ≥ 3 force extension cycles. (H and I) Fitted rate of nucleosome opening increases with either FACT or subunit HMGB, consistent with histone DNA destabilization, while MD only weakly induces destabilization. Errors determined from fitting.

(J) Summary of the measured changes in the nucleosome free energy landscape (gray) in the presence of FACT (green), HMGB (blue), or MD (red), where the outer half wraps are no longer evident (using Equations 6–8). Values of the binding affinities are in Table S1 and the parameters characterizing the stability of the nucleosome are summarized in Table S2.

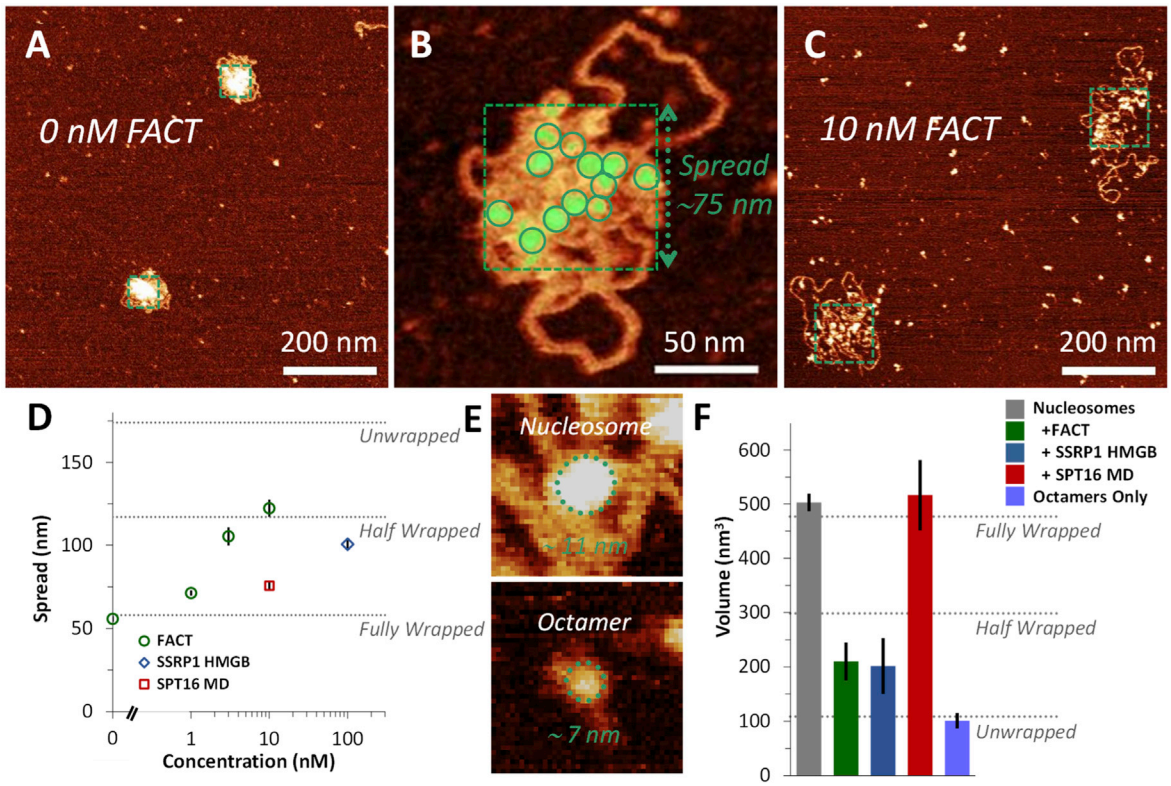

Figure 4. Nucleosome unwinding from AFM imaging

(A) Nucleosome arrays imaged using AFM, highlighting two distinct (non-interacting) arrays.

(B) Higher resolution shows ~12 octamers on each array (bright spots/regions highlighted by circles) remain in close proximity. Quantifying this spread as a minimum square that contains all the observed nucleosomes in an array (dotted green line, see Figure S6 for typical height profiles and threshold details).

(C) Partial unwrapping of the DNA mediated by FACT results in a longer effective DNA linker between each histone octamer, leading to larger spreads (green).

(D) Measured average spread of histones per array as a function of full FACT concentration (green), and in the presence of SSRP1 HMGB (blue) and SPT16 MD (red). Dotted lines (gray) indicate values of the spread that correspond to fully, partially, and completely unwrapped nucleosomes, as described in the text and the supplemental information. Full FACT and the two domains lead to unwrapping of the DNA from the octamer.

(E) Image of a full nucleosome and an isolated octamer, highlighting the measured volumes, determined from thresholds described in STAR Methods and shown in Figure S5.

(F) In the presence of FACT or HMGB, the measured spread increases, as nucleosomes are less wrapped when DNA is released from the octamer. Subunit MD does not lead to measurable loss. All errors are SEM.

interaction energy of the core decreased significantly with the addition of either full FACT or SSRP1 HMGB. However, isolated SPT16 MD subunits lead to an increase in both the barrier height and overall energy of DNA-core interactions. These results are summarized in comparison with protein-free nucleosomes in Figure 3J and are quantified in Table S2.

AFM images of FACT effects on nucleosome array order

Direct AFM images of nucleosome arrays in liquid highlight the extent of nucleosome arrays (Figure 4A). Utilizing a method to facilitate rapid sample preparation[57] and fast liquid scanning tips, detailed images allow specific height analysis. While individual nucleosomes are resolved (Figure 4B), the unbiased random walk observed for the DNA path cannot be reliably traced through the full array. Furthermore, individual nucleosomes become more difficult to distinguish as FACT is added. To quantify these images, an effective area of array "spread" can be defined (green box in Figure 4B), drawn around a height threshold of 2 nm that captures all histones in the array (shown in Figure S5). Nucleosome arrays used in these experiments, with a fixed spacing of 60 bp (Figure 1H), produce a specific value of the spread (validated through polymer modeling, in Figure S5). Larger values of the spread correspond to longer lengths of DNA between nucleosomes (Figure 4C). Arrays exposed to FACT have a larger spread value due to DNA release from the nucleosome. The spread increases with increasing concentrations of FACT or with saturating concentrations of SSRP1 HMGB and SPT16 MD (Figure 4D). These results indicate that the two combined isolated domains of FACT bind to nucleosomes and promote release of the outer half wraps of DNA independently, confirming the OT results above (Figures 3D and 3F).

Several array images reveal isolated nucleosomes along the DNA. These cases were rare and found for limiting conditions, including zero or high FACT concentrations ($\geq$10 nM for AFM conditions). Nucleosome area and volume were estimated in

these cases, with the most consistent results for an imaging height threshold of 2 nm. Nucleosome height profiles revealed a shape best described by a flattened ellipsoid, and this shape yielded an intact nucleosome volume of 500 ± 20 nm^3 and a volume of 101 ± 14 nm^3 for isolated histone octamers in the absence of any DNA (Figures 4E and 4F). These values are in agreement with a theoretical nucleosome diameter of 11 nm and height of 5 nm,[1,3] predicting a volume of ~470 nm^3, and a theoretical histone octamer diameter of 7 nm and height of 3 nm[1,3] predicting a volume of ~115 nm^3. These estimates are shown as dotted lines for fully wound and unwound nucleosomes in Figure 4F. Importantly, the measured volumes do not consider the AFM tip volume, and the assumption of a continuous geometry may lead to missing volume, especially below the height threshold (see Figure S5). Addition of 10 nM FACT might be expected to yield an increase in the measured volume of the FACT-nucleosome complex as the 220-kDa FACT assembly is similar in mass to the 100-kDa histone octamer with its 100 kDa of wrapped DNA. However, the measured volume of FACT-treated nucleosomes is only 210 ± 30 nm^3 (Figure 4F). This volume deficit is likely due to unwinding of the outer wrap of nucleosomal DNA upon FACT remodeling (and FACT is probably not bound). Furthermore, it is likely that protein is lost from the octamer as FACT unbinds before imaging, although it is possible that the remodeled octamer is no longer complete, as we cannot resolve dimer loss in these images. Quantitatively, these results are most consistent with an intact octamer and less wound DNA. Finally, while exposure to SSRP1 HMGB also results in DNA loss comparable with full FACT, exposure to SPT16 MD results in no measurable loss, despite the unwinding seen in OT experiments above.

Nucleosome remodeling revealed by fluorescence imaging

To monitor nucleosome disruption kinetics, a variation of the construct in Figure 2A was developed for single-molecule imaging (shown in Figure 5A). The 1,350-bp flanking DNA handles were replaced by 3,000-bp handles and the digoxygenin label was replaced with a second biotin. Imaged nucleosomes can thus be distinguished from bead autofluorescence. Fluorescent dyes were conjugated at cysteine substitutions (T112C) in each H2B monomer, yielding two fluorophores per nucleosome (Alexa488 or Atto647N, Figure 5A), assembled in a microfluidics chamber (Figure 5B). Confocal imaging at a constant 1 pN of stretching force (Figure 5C) reveals nucleosome arrays. At this force, intact nucleosomes of 11 nm diameter will be separated by 60-bp linkers. The total length of the array can be estimated to be ~350 nm. Extending such an array with 40 pN of force (Figure 5D) leads to the disruption of both inner and outer DNA wraps, with a total theoretical extension length of ~800 nm. At 1 pN stretching force, measured extensions of these fluorescent structures (above a background threshold) reveal a length along the connecting DNA of 420 ± 20 nm, somewhat longer than predicted, likely influenced by the diffraction limit of the instrument ($\lambda/2NA$). At 40 pN, the measured value of 800 ± 20 nm more closely matches the expected value. Notably, although the DNA is completely unwrapped from the histone octamer under these conditions, the central dyad of the $(H3\text{-}H4)_2$ tetramer remains attached to the DNA for some time, in agreement with recent observations.[58]

Arrays were disrupted by stretching force and held at a fixed tension of 40 pN to monitor loss of disrupted octamers. Kymographs at this tension revealed that the extension of the arrays increased during disruption (Figure 5E), as expected from confocal imaging. Over several minutes, intensity was gradually lost as histones were released into solution. As the fluorescent labels are tethered to the H2A histone, these images directly reveal the release of the of the H2A/H2B dimers. Evidence presented below strongly suggests immediate or rapid loss of all remaining histones follows. Repeating these experiments in the presence of saturating concentrations of full FACT revealed a distinct increase in this release rate (Figure 5F). Finally, comparisons with SSRP1 HMGB and SPT16 MD show that complete FACT induced the most rapid octamer release. Single exponential fits to the release data are shown in Figure 5G and averaged results are shown in Figure 5H and in Table S1. The rates are corrected for the measured loss of signal due to photobleaching as described in STAR Methods. Overall, the disruption induced by full FACT or FACT subunit binding to the nucleosome leads directly to rapid release of the octamer from the DNA, with full FACT driving the most rapid release.

Nucleosome chaperone activities of SSRP1 HMGB and SPT16 MD

After tension-induced disruption of histone-DNA interactions, inner wrap DNA remains in contact with the histone octamer core at the central dyad site, and these bound histone octamers persist over several minutes during DNA stretch and release cycles, allowing fractional reformation of the nucleosome array in each cycle. Under standard conditions (10 mM HEPES, 100 mM NaCl [pH 7.5]), individual nucleosomes have been observed to reform for ~5 cycles after disruption, with each cycle lasting ~10 s, and individual disruptions lasting <5 s (Figure 6A). In saturating conditions of FACT, disruption/reformation is observed for well over 10 cycles (Figure 6B). The number of inner wrap releases (Figure 6C), and corresponding forces (Figure 6D), and length of wrapped DNA (Figure 6E), can be measured in these "survival probability" experiments. In contrast, the outer wrap release force was not reliably observed. In nearly all cases, surviving nucleosomes appear to release with slightly less force as the number of cycles increases and the surviving number decreases. Interestingly, this is the opposite of the prediction for arrays of fully wrapped nucleosomes (Equation 2), where an array with fewer nucleosomes releases each surviving nucleosome at higher force due to the effectively higher stretching rate. This is, indeed, observed in the average release force for each subsequent force peak upon the first stretch of our nucleosome array (Figure 2E). We interpret this decrease in strong site release force over repeated stretching cycles as evidence that disrupted nucleosomes do not fully re-form upon construct relaxation. The length of DNA released in subsequent cycles (the length wrapped after the previous disruption/relaxation) decreases as well (Figure 6E), although only by a few base pairs. Overall, octamers become dislocated from optimal wrapping positions, and possibly displaced from each other, as the core sites are present if not optimally assembled. After the loss of the

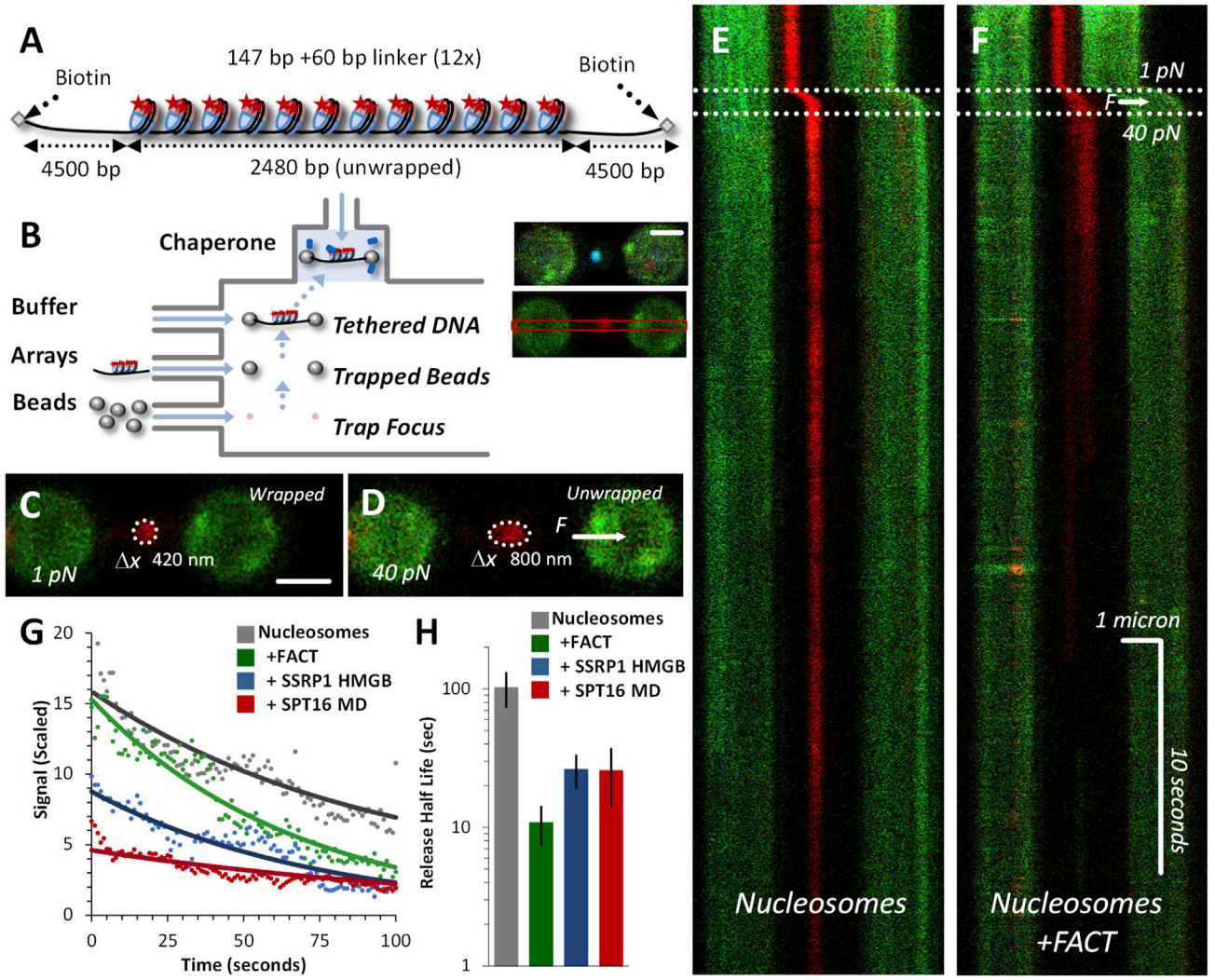

Figure 5. Visualizing nucleosome disruption under tension and FACT-driven octamer loss

(A) A 12× nucleosome array incorporates fluorescent labels (Alexa488 or Atto647N) on each H2B (T112C) during reconstitution.

(B) Arrays are assembled in parallel flow channels and observed in a LUMICKS C-Trap confocal microscope. Scale bar, 1 μm.

(C and D) Under increasing tension, confocal images of the array elongate as DNA is unwound from the octamer. Images are diffraction limited in (C), but the overall length of unwound nucleosomes is evident in (D). Scale bar, 1 μm.

(E) Kymographs confirm that, although a tension of 40 pN completely unwinds the nucleosomes, surviving histone octamers are only slowly lost to solution. The inset to (B) shows the kymograph scanning area in the red box.

(F) The presence of full FACT increases the rate of loss. Scale bars, 1 μm and 10 s.

(G) Fitted fluorescence decay for disrupted nucleosomes (gray) and in the presence of full FACT (green), SSRP1 HMGB (blue, and SPT16 MD (red).

(H) Summary of fitted rates reveals the fastest release from the DNA occurs in the presence of the full protein (n ≥ 3 and errors are SEM).

"ripping" events over 10 cycles, no evidence of protein binding remains.

Remarkably, intact FACT displays dramatic nucleosome chaperone activity. Nucleosomes may be disrupted and reformed for up to 30 cycles (Figures 6C–6E). Reformation occurs despite the destabilizing activity induced by FACT binding (Figure 6D). FACT binding simultaneously weakens histone-DNA interactions and chaperones their reformation after force disruption. In contrast, the separate subunits do not exhibit this activity. Exposure of nucleosome arrays to the SSRP1 HMGB domain decreased both the probability of reformation in each cycle and the stability of the reformed nucleosomes over stretching cycles (Figures 6C and 6D). This is consistent with a protein that binds to nucleosomal DNA, weakening histone-DNA contacts and preventing complete restoration of the wrapped structure after the release of force.[18,49] Rapid and complete loss of measured DNA-histone interactions, coupled with the loss of fluorescence signal from the dimers discussed above strongly suggest the loss of the entire octamer to solution when HMGB bound nucleosomes are disrupted by tension. The SPT16 MD domain increases the force required to disrupt nucleosomes, with small effects on survival

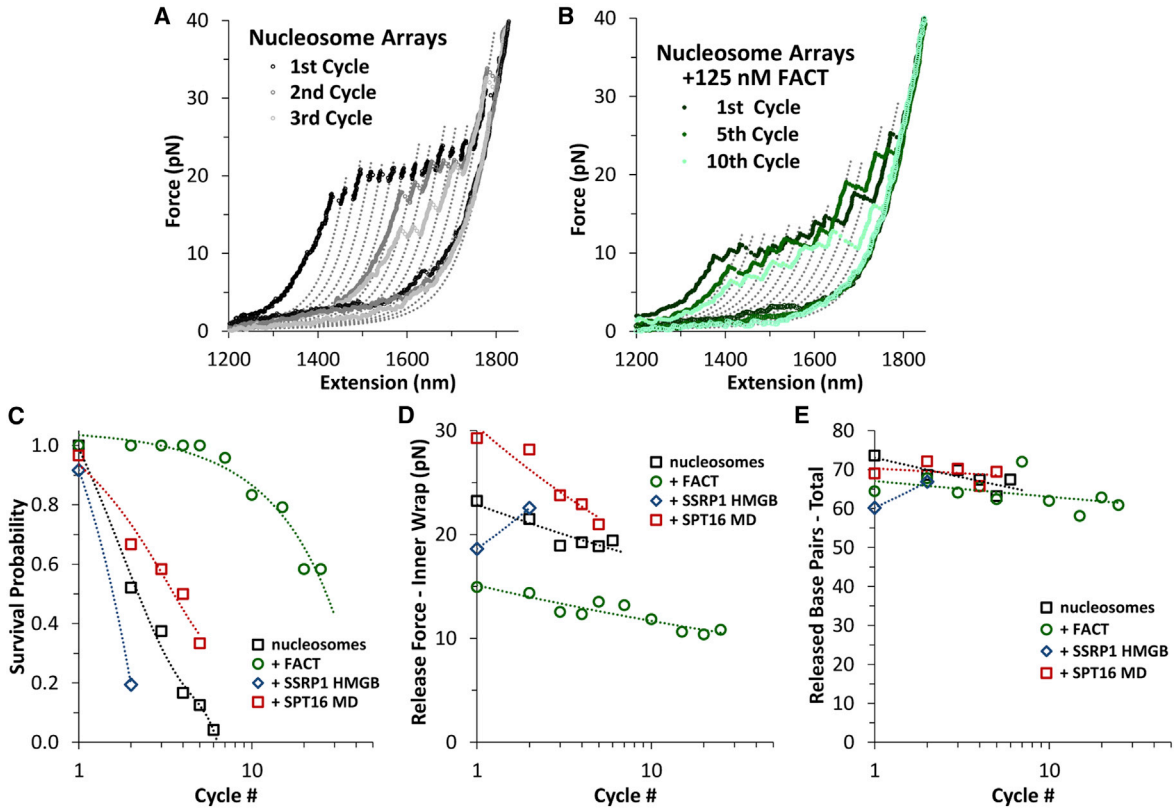

Figure 6. FACT catalysis: Destabilizing and reassembling nucleosomes

(A) Sequences of force extension/disruption and release/reformation (black, charcoal, and gray). The releases characterized in Figure 3 may be measured again across multiple cycles, although diminishing numbers of nucleosomes reform. Dotted lines reflect the contour length of arrays separated by the length of a single disrupted nucleosome (Equation 1).

(B) Arrays in the presence of FACT are disrupted with less force, but reform over dozens of cycles (forest, green, teal).

(C and D) (C) Measured survival probabilities for an individual nucleosome increases dramatically in the presence of saturating conditions of FACT, although (D) nucleosomes release with lower force.

(E) The released length appears nearly unchanged, indicating that the core sites remain, even though the nucleosome does not completely reassemble with each cycle of disruption. Isolated SSRP1 HMGB domains (blue), by contrast, destabilize nucleosomes and do not facilitate reformation. Although SPT16 MD (red) initially stabilize nucleosomes, this subunit also does not facilitate reformation. Only full FACT is competent to catalyze both nucleosome disassembly and reassembly. For all graphs, n $\geq$ 3 arrays (except for FACT, where n = 2).

probability (Figures 6C–6E). This effect resembles native nucleosomes in low (50 mM) cation. The SPT16 MD domain can thus stabilize nucleosome core sites without facilitating nucleosome reformation as force is relaxed. Importantly, the MD domain used here does not include the CTD, known to tether the H2A/H2B dimer to the remaining structure.[6,16] Thus, FACT domains must coordinate to enhance accessibility of nucleosomal DNA while mediating rapid histone-DNA fluctuations to facilitate DNA rewrapping. Crucially, the data presented here suggest that FACT, having remodeled the nucleosome, remains bound upon the increase and release of tension over these many cycles (the disrupted form remains so only for <5 s in these experiments). The bound protein both chaperones nucleosome reformation as tension is released while maintaining the weakened histone-DNA interactions seen in each subsequent cycle. Thus, FACT binding facilitates both complete octamer loss for disrupted nucleosomes and rapid nucleosome reformation as tension is released.

DISCUSSION

Tension disrupts nucleosomes while preserving histone octamers on DNA

We observe that tension disrupts DNA-histone contacts (Figure 7A), confirming earlier single-molecule studies.[2,18,59] This includes the gradual loss of weaker contacts between the histones and the outer half wraps of DNA. This disruption is followed by the more sudden release of stronger DNA contacts with the histones of the H2A/H2B dimers and $(H3\text{-}H4)_2$ tetramer—the "strong" sites (Figure 2). The central dyad of the $(H3\text{-}H4)_2$ tetramer then appears to remain in contact with DNA and increased tension does not effectively dissociate remaining histones from the DNA. Our survival probability experiments (Figure 6) show that, as tension is released, approximately half of nucleosomes reform. Furthermore, experiments with fluorescently labeled histone H2A/H2B dimers show that disruption does not immediately lead to H2A/H2B dimer or octamer loss,

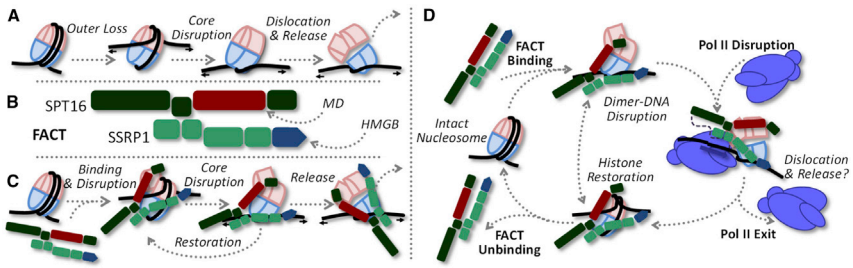

Figure 7. Hypothetical FACT subdomain roles during transcription

(A) Cartoon of nucleosome release under tension, including DNA-histone disruption from the strong sites, releasing DNA up to the strong sites and the central dyad. Core H2A/H2B dimer and $(H3\text{-}H4)_2$ tetramer-DNA contacts, although weakened, remain intact. Histone loss is not immediate, and displacement of these contacts may inhibit nucleosome restoration even without loss, which ultimately occurs if disruption is maintained.

(B) Heterodimeric FACT structure (green/forest) highlights functional subunits MD of SPT16 (red) and HMGB of SSRP1 (blue).

(C) FACT catalyzes both nucleosome destabilization and reassembly during cycles of force-induced disruption during tweezers experiments. While the SPT16 MD strengthens core histone-DNA interactions, the SSRP1 HMGB domain disrupts DNA-histone interactions throughout the nucleosome. Together, these domains tether disrupted histones to DNA, resisting displacement and providing an increased pathway for nucleosome reformation.

(D) Proposed model of the role of full FACT in transcription by polymerase II. Full FACT binding disrupts the nucleosome via H2A/H2B displacement, enhancing RNAP access. After polymerase-induced dislocation, full FACT catalyzes nucleosome reassembly. FACT-bound nucleosomes may undergo multiple rounds of polymerase elongation before FACT dissociates, restoring the nucleosome.

in agreement with earlier experiments (although the labels there were not specific to the dimers).[58] We propose that while surviving octamers remain bound to extended DNA, many are sufficiently rearranged to inhibit efficient reformation. Rearrangement may include either (or both) significant DNA dislocation along the central dyad or dislocation of histones from within the octamer.

FACT SSRP1 HMGB binds to entry/exit DNA, while FACT SPT16 MD binds both DNA and histones

Full FACT binding clearly weakens DNA-histone interactions, driving the loss of the two outer half wraps of DNA (Figures 3 and 5). Strong site interactions are significantly weakened by full FACT as well, requiring less force to disrupt. Overall, the stabilizing energy of DNA-histone contacts decreases by approximately half (Table S1). We find that the individual SSRP1 HMGB and SPT16 MD domains independently affect core sites (Figure 3B), while little direct interaction of other FACT subunits with the nucleosome was observed up to $\sim$ 250 nM concentration (Figures 3A and 3B). Yet, while SSRP1 HMGB and SPT16 MD domains both bind the nucleosome, they affect the nucleosome in distinct ways.

Addition of the isolated FACT HMGB domain leads to extensive unwinding of DNA from the nucleosome, as outer wrap DNA interactions can be completely destabilized, and inner wrap interactions are weakened to about a half of their original stability. Considering our previous studies of HMGB proteins on nucleosome stability,[18] as well as complementary studies of single nucleosomes with FACT,[12] we conclude that, in the context of FACT, HMGB domains reduce nucleosome stability by analogy with free HMGB proteins, although the FACT HMGB domain displays a weaker effect than the HGMB domain of *Saccharomyces cerevisiae* Nhp6A.[49] Thus, we attribute most of the nucleosome destabilization activity of FACT to HMGB domain binding at the nucleosome DNA entry and exit points, kinking the DNA at those sites and destabilizing histone interactions as seen previously for HMGB domains[18,60] and much as conjectured.[61,62] However, the HMGB domain also tethers the bound DNA outer wrap to the full protein and the remainder of the octamer. While this tethering activity is consistent with the measurements in a previous single-molecule study, those authors attributed to this domain a role in stabilizing the nucleosome,[12] whereas here we see a clear destabilizing effect by HMGB binding.

In contrast, we observe SPT16 MD stabilizing the nucleosome core sites, as detected by increased core site release force, binding and transition state free energies, and the lack of zero-force opening rate enhancement, relative to the values of these parameters in the presence of full FACT (Tables S1 and S2). This result is consistent with recent cryo-EM studies,[6] where nucleosomes lacking the outer DNA wraps preserved H2A/H2B dimer binding via interaction with domains of SPT16 (the SSRP1 HMGB domain was not present in this structure). Our results also suggest that SPT16 MD simultaneously binds the octamer and wrapped DNA. A single SPT16 MD domain can stabilize core strong site interactions (Figure 3J) while simultaneously driving the release of outer wrapped DNA up to the dimers, as also predicted and seen in recent structures.[6,15] Our force disruption experiments did not see strong evidence of isolated SPT16 CTD domain binding to the H2A/H2B dimer, apparent in those results.[6,15] This may mean that the MD and CTD domains coordinate and the disorganized CTD domain is unable to function effectively on its own. The ability of the SPT16 MD domain to tether parts of the nucleosome is more pronounced in the context of full FACT, and recent studies have shown that the SPT16 CTD tail serves an important role in H2A/H2B dimer tethering (Figure 1)[5,6,16] and our full FACT includes this SPT16 CTD domain.

Our results thus characterize the coordinated functions of FACT wherein individual subdomains bind to various components of the nucleosome, competing with histone-histone and histone-DNA interactions (Figures 7B and 7C). Binding leads to partial nucleosome destabilization, which becomes more profound in the presence of applied stress through unwinding forces generated experimentally by motor proteins, such as polymerases. Nonetheless, the same FACT subdomains that competitively bind nucleosome components during destabilization also tether these nucleosome components, enhancing nucleosome reassembly after the removal of external stress (Figure 7D). Critically, only the combined effects of SSRP1 HMGB

and SPT16 MD (and likely CTD) effectively tether disrupted histone to the DNA.

FACT tethers histones to DNA

Our survival probability experiments, and images of labeled nucleosomes, give more insight into the roles of FACT and its subunits in tethering nucleosome components. Our fluorescence visualization experiments suggest that the isolated subdomains HMGB and MD increase the release of the central histone dyad that remains attached to DNA. Surprisingly, full FACT protein induces the fastest release of the disrupted octamer from the DNA. Yet this is consistent with experiments above, which showed that FACT destabilizes histone-DNA contacts throughout the nucleosome (lower average core site release force; Figures 3B and 6D), while increasing the kinetics of DNA-histone opening (Figures 3H and 3I). With this in mind, we repeated the stretch/release cycle in the presence of full FACT to keep the disruption time below the measured disrupted half-life. Yet, while native arrays did not reliably reform after a few cycles, the presence of FACT led to the nearly complete restoration of core site interactions with DNA (Figure 6). Thus, FACT chaperones histone-DNA interactions and inhibits octamer dislocation and loss, consistent with previous observations.[12,20] FACT facilitates the unwrapping and rewrapping of DNA around the core sites of the octamer as force is applied and released over 30 cycles. Within FACT, the two principal domains studied here individually disrupt or maintain DNA-histone interactions, while neither can function independently to prevent loss of the histones from the disrupted nucleosome (Figure 5H). This reveals necessary coordination between these two protein subunits. Furthermore, in the full protein, other subunits likely contribute to nucleosome reorganization and tethering (particularly the SPT16 CTD domain as discussed above). Ultimately, survival probability and measured release force both decrease as the number of disruptions increases (Figure 6), indicating that multiple rounds of disruption eventually lead to vhistone disorganization, and then eventual loss.

FACT catalyzes histone reorganization on DNA

Full FACT significantly destabilizes the nucleosome such that the free energy of DNA/histone interactions in its presence constitutes only 57% of its native stability in 100 mM NaCl (Table S2). However, the destabilizing effect of FACT on the nucleosome transition state appears even more pronounced, leading to a 3-fold reduction in the disruption transition barrier free energy (Figure 3J). Thus, in a formal sense, FACT activity is catalytic, enhancing the probability of both nucleosome wrapping and unwrapping. Catalysis is achieved by binding to and stabilizing the partially unwrapped transition state. This stabilization is achieved by substituting disrupted inter-histone and histone-DNA interactions with competitive interactions involving these DNA and histone sites and FACT domains. The dynamic nature of FACT binding and FACT-catalyzed rate enhancement for nucleosome wrapping and unwrapping chaperones polymerase passage through nucleosomes.

Force-induced nucleosome disruption provides insights into the likely response of nucleosomes to the passage of RNAPs (Figure 7D), as discussed previously,[17] and revealed in a recent sequence of cryo-EM structures.[63] FACT binding disrupts the intact nucleosome, as FACT subunits bind to histones and DNA, competing with histone-DNA interactions. This weakening of intra-nucleosome interactions facilitates the passage of RNAPs, which may further dislocate histones, and even lead to histone loss. Yet, FACT simultaneously tethers dislocated histones, minimizing histone loss. Intriguingly, the fast kinetics of histone-FACT-DNA interactions suggest that Pol-induced disruption must be short lived, or that disruption may be processive, as also suggested in a recent cryo-EM study.[63] After polymerase translocation, nucleosome components may be restored to a partially disrupted state, facilitating passage of another RNAP. FACT may also unbind, returning the nucleosome to a fully intact state, and may collaborate with other nuclear chaperones in this process. Minimizing accumulation of deleterious free histones highlights another role of FACT.

Conclusions

In this work, we show that FACT not only enhances transcription by disrupting the nucleosome but facilitates the reorganization of the nucleosome by tethering the displaced histone to the DNA. FACT achieves this through the coordinated activity of two key domains that affect the nucleosome in differing ways. The HMGB domain of the SSRP1 subunit binds DNA, dislocating the outer wraps from the octamer, destabilizing all DNA-histone contacts throughout the nucleosome, and increasing the kinetics of nucleosomal fluctuations and even loss during disruption. The SPT16 MD domain stabilizes the core even while driving the loss of the outer half wraps of DNA from the nucleosome. Critically, both domains increase the kinetics of DNA-histone interactions, as does the full protein. Yet the divergent activities of the two major subunits of FACT combine with contacts throughout the protein to both destabilize the nucleosome, facilitating the passage of polymerases, while also performing the seemingly contradictory function of facilitating nucleosome reassembly. Thus, FACT catalyzes nucleosome transactions.

Limitations of the study

All the human FACT constructs used in our manuscript were produced in *E. coli* and purified to homogeneity. However, using expression in *E. coli*, we were unable to successfully purify FACT with SPT16 NTD and SSRP1 CTD to homogeneity, as these segments are flexible and prone to degradation. We are currently working on purifying full-length FACT.

In this work, the effectiveness of an isolated domain was compared with the whole across several types of single-molecule experiments. This approach was particularly fruitful for domains that had some secondary structure, including SPT16 MD, or function well isolated *in vivo*, including SSRP1 HMGB. However, this approach was less useful for highly disorganized domains, such as SPT16 CTD, which showed only modest effects on nucleosome stability, despite a known role in binding the H2A/H2B dimer, as detailed in the introduction and the discussion above. In future work, a domain consisting of SPT16 MD + CTD would be useful to study in comparison with the work shown here.

Confocal and kymograph fluorescence data, coupled with the survival probability experiments, make a convincing case for

nucleosome dislocation and octamer loss, as accelerated by key FACT domains. However, as pointed out in the results and discussion, fluorescent labels are located only on the H2B histones of each dimer. More direct and useful kinetic information on unbinding would be obtained by relocating the label to the tetramer and checking unbinding in comparison with these data. In addition, a label placed directly on the binding proteins would allow simultaneous observation of protein binding/unbinding, histone-DNA disruption, and histone loss.

STAR★METHODS

Detailed methods are provided in the online version of this paper and include the following:

- KEY RESOURCES TABLE
- RESOURCE AVAILABILITY
  - Lead contact
  - Materials availability
  - Data and code availability
- METHOD DETAILS
  - Preparation of DNA constructs
  - Octamer assembly onto DNA
  - Preparation/purification of recombinant FACT and FACT domain protein
  - Dual beam optical tweezers
  - AFM imaging in liquid
  - Combined fluorescence and optical tweezers
- QUANTIFICATION AND STATISTICAL ANALYSIS
  - Modeling dsDNA elasticity
  - Identifying DNA release from the force extension data
  - Determining forces and the kinetics of strong site disruption
  - Measuring DNA lengths released from nucleosome strong sites of the core
  - Quantifying protein-nucleosome binding through variations in the force driving inner wrap release
  - Quantifying protein-DNA binding through variations in the dsDNA persistence length
  - Calculating the energy of histone-DNA disruption
  - Measuring the energy barrier of inner wrap disruption
  - AFM image analysis
  - Confocal/Kymograph image analysis
  - Correction to measured lifetimes due to photobleaching

SUPPLEMENTAL INFORMATION

Supplemental information can be found online at https://doi.org/10.1016/j.celrep.2022.111858.

ACKNOWLEDGMENTS

This research was funded by National Science Foundation grant MCB-1817712 (to M.C.W.), and funding for a shared instrument used in this research was provided by National Science Foundation grant DBI-1828506. Additional funding included Howard Hughes Medical Institute and National Institutes of Health grant NCI R01CA218255 (to K.L.), National Institutes of Health NIGMS grant R35 GM136262 (to G.M.), and funding from the Mayo Clinic (to L.J.M.).

AUTHOR CONTRIBUTIONS

Q.H. and M.V.B. cloned and purified the different FACT constructs in the lab of G.M. U.M.M. synthesized octamers, including the labeled octamers in the lab of K.L. N.B. labeled and purified DNA constructs for array positioning in the lab of L.J.M. M.J.M. reconstituted the octamers onto the DNA constructs, conducted the OT and SMF experiments, and analyzed the data in the lab of M.C.W. M.M., E.N., and R.H. performed AFM experiments, and M.M. analyzed the data and conducted modeling. M.J.M., I.R., M.C.W., L.J.M., G.M., and K.L. wrote/edited the manuscript.

DECLARATION OF INTERESTS

The authors declare no competing interests.

Received: July 27, 2022
Revised: October 6, 2022
Accepted: November 30, 2022
Published: December 27, 2022

REFERENCES

1. Luger, K., Mäder, A.W., Richmond, R.K., Sargent, D.F., and Richmond, T.J. (1997). Crystal structure of the nucleosome core particle at 2.8 A resolution. Nature *389*, 251–260.
2. Brower-Toland, B.D., Smith, C.L., Yeh, R.C., Lis, J.T., Peterson, C.L., and Wang, M.D. (2002). Mechanical disruption of individual nucleosomes reveals a reversible multistage release of DNA. Proc. Natl. Acad. Sci. USA *99*, 1960–1965. https://doi.org/10.1073/pnas.022638399.
3. Davey, C.A., Sargent, D.F., Luger, K., Maeder, A.W., and Richmond, T.J. (2002). Solvent mediated interactions in the structure of the nucleosome core particle at 1.9Å resolution. J. Mol. Biol. *319*, 1097–1113. https://doi.org/10.1016/s0022-2836(02)00386-8.
4. Farnung, L., Ochmann, M., Engeholm, M., and Cramer, P. (2021). Structural basis of nucleosome transcription mediated by Chd1 and FACT. Nat. Struct. Mol. Biol. *28*, 382–387. https://doi.org/10.1038/s41594-021-00578-6.
5. Mayanagi, K., Saikusa, K., Miyazaki, N., Akashi, S., Iwasaki, K., Nishimura, Y., Morikawa, K., and Tsunaka, Y. (2019). Structural visualization of key steps in nucleosome reorganization by human FACT. Sci. Rep. *9*, 10183. https://doi.org/10.1038/s41598-019-46617-7.
6. Liu, Y., Zhou, K., Zhang, N., Wei, H., Tan, Y.Z., Zhang, Z., Carragher, B., Potter, C.S., D'Arcy, S., and Luger, K. (2020). FACT caught in the act of manipulating the nucleosome. Nature *577*, 426–431. https://doi.org/10.1038/s41586-019-1820-0.
7. Ohndorf, U.-M., Rould, M.A., He, Q., Pabo, C.O., and Lippard, S.J. (1999). Basis for recognition of cisplatin-modified DNA by high-mobility-group proteins. Nature *399*, 708–712.
8. Formosa, T. (2008). FACT and the reorganized nucleosome. Mol. Biosyst. *4*, 1085–1093. https://doi.org/10.1039/b812136b.
9. Reinberg, D., and Sims, R.J., 3rd. (2006). De FACTo nucleosome dynamics. J. Biol. Chem. *281*, 23297–23301. https://doi.org/10.1074/jbc.R600007200.
10. Singer, R.A., and Johnston, G.C. (2004). The FACT chromatin modulator: genetic and structure/function relationships. Biochem. Cell. Biol. *82*, 419–427. https://doi.org/10.1139/o04-050.
11. Winkler, D.D., and Luger, K. (2011). The histone chaperone FACT: structural insights and mechanisms for nucleosome reorganization. J. Biol. Chem. *286*, 18369–18374. https://doi.org/10.1074/jbc.R110.180778.
12. Chen, P., Dong, L., Hu, M., Wang, Y.Z., Xiao, X., Zhao, Z., Yan, J., Wang, P.Y., Reinberg, D., Li, M., et al. (2018). Functions of FACT in breaking the nucleosome and maintaining its integrity at the single-nucleosome level. Mol. Cell *71*, 284–293.e4. https://doi.org/10.1016/j.molcel.2018.06.020.

13. Gurova, K., Chang, H.W., Valieva, M.E., Sandlesh, P., and Studitsky, V.M. (2018). Structure and function of the histone chaperone FACT - resolving FACTual issues. Biochimica et Biophysica Acta - Gene Regulatory Mechanisms *1861*, 892–904. https://doi.org/10.1016/j.bbagrm.2018.07.008.

14. Wang, T., Liu, Y., Edwards, G., Krzizike, D., Scherman, H., and Luger, K. (2018). The histone chaperone FACT modulates nucleosome structure by tethering its components. Life Sci. Alliance *1*, e201800107. https://doi.org/10.26508/lsa.201800107.

15. Tsunaka, Y., Fujiwara, Y., Oyama, T., Hirose, S., and Morikawa, K. (2016). Integrated molecular mechanism directing nucleosome reorganization by human FACT. Genes Dev. *30*, 673–686. https://doi.org/10.1101/gad.274183.115.

16. Kemble, D.J., McCullough, L.L., Whitby, F.G., Formosa, T., and Hill, C.P. (2015). FACT disrupts nucleosome structure by binding H2A-H2B with conserved peptide motifs. Mol. Cell *60*, 294–306. https://doi.org/10.1016/j.molcel.2015.09.008.

17. McCullough, L.L., Connell, Z., Xin, H., Studitsky, V.M., Feofanov, A.V., Valieva, M.E., and Formosa, T. (2018). Functional roles of the DNA-binding HMGB domain in the histone chaperone FACT in nucleosome reorganization. J. Biol. Chem. *293*, 6121–6133. https://doi.org/10.1074/jbc.RA117.000199.

18. McCauley, M.J., Huo, R., Becker, N., Holte, M.N., Muthurajan, U.M., Rouzina, I., Luger, K., Maher, L.J., 3rd, Israeloff, N.E., and Williams, M.C. (2019). Single and double box HMGB proteins differentially destabilize nucleosomes. Nucleic Acids Res. *47*, 666–678. https://doi.org/10.1093/nar/gky1119.

19. Stillman, D.J. (2010). Nhp6: a small but powerful effector of chromatin structure in Saccharomyces cerevisiae. Biochim. Biophys. Acta *1799*, 175–180. https://doi.org/10.1016/j.bbagrm.2009.11.010.

20. Valieva, M.E., Armeev, G.A., Kudryashova, K.S., Gerasimova, N.S., Shaytan, A.K., Kulaeva, O.I., McCullough, L.L., Formosa, T., Georgiev, P.G., Kirpichnikov, M.P., et al. (2016). Large-scale ATP-independent nucleosome unfolding by a histone chaperone. Nat. Struct. Mol. Biol. *23*, 1111–1116. https://doi.org/10.1038/nsmb.3321.

21. Hondele, M., and Ladurner, A.G. (2013). Catch me if you can: how the histone chaperone FACT capitalizes on nucleosome breathing. Nucleus *4*, 443–449. https://doi.org/10.4161/nucl.27235.

22. Belotserkovskaya, R., Oh, S., Bondarenko, V.A., Orphanides, G., Studitsky, V.M., and Reinberg, D. (2003). FACT facilitates transcription-dependent nucleosome alteration. Science *301*, 1090–1093. https://doi.org/10.1126/science.1085703.

23. Garcia, H., Fleyshman, D., Kolesnikova, K., Safina, A., Commane, M., Paszkiewicz, G., Omelian, A., Morrison, C., and Gurova, K. (2011). Expression of FACT in mammalian tissues suggests its role in maintaining of undifferentiated state of cells. Oncotarget *2*, 783–796. https://doi.org/10.18632/oncotarget.340.

24. Hertel, L., De Andrea, M., Bellomo, G., Santoro, P., Landolfo, S., and Gariglio, M. (1999). The HMG protein T160 colocalizes with DNA replication foci and is down-regulated during cell differentiation. Exp. Cell Res. *250*, 313–328. https://doi.org/10.1006/excr.1999.4495.

25. Lolas, I.B., Himanen, K., Grønlund, J.T., Lynggaard, C., Houben, A., Melzer, M., Van Lijsebettens, M., and Grasser, K.D. (2010). The transcript elongation factor FACT affects Arabidopsis vegetative and reproductive development and genetically interacts with HUB1/2. Plant J. *61*, 686–697. https://doi.org/10.1111/j.1365-313X.2009.04096.x.

26. Safina, A., Garcia, H., Commane, M., Guryanova, O., Degan, S., Kolesnikova, K., and Gurova, K.V. (2013). Complex mutual regulation of facilitates chromatin transcription (FACT) subunits on both mRNA and protein levels in human cells. Cell Cycle *12*, 2423–2434. https://doi.org/10.4161/cc.25452.

27. LeRoy, G., Oksuz, O., Descostes, N., Aoi, Y., Ganai, R.A., Kara, H.O., Yu, J.R., Lee, C.H., Stafford, J., Shilatifard, A., and Reinberg, D. (2019). LEDGF and HDGF2 relieve the nucleosome-induced barrier to transcription in differentiated cells. Sci. Adv. *5*, eaay3068. https://doi.org/10.1126/sciadv.aay3068.

28. Martin, B.J.E., Chruscicki, A.T., and Howe, L.J. (2018). Transcription promotes the interaction of the FAcilitates chromatin transactions (FACT) complex with nucleosomes in Saccharomyces cerevisiae. Genetics *210*, 869–881. https://doi.org/10.1534/genetics.118.301349.

29. Gasparian, A.V., Burkhart, C.A., Purmal, A.A., Brodsky, L., Pal, M., Saranadasa, M., Bosykh, D.A., Commane, M., Guryanova, O.A., Pal, S., et al. (2011). Curaxins: anticancer compounds that simultaneously suppress NF-κB and activate p53 by targeting FACT. Sci. Transl. Med. *3*, 95ra74. https://doi.org/10.1126/scitranslmed.3002530.

30. Koman, I.E., Commane, M., Paszkiewicz, G., Hoonjan, B., Pal, S., Safina, A., Toshkov, I., Purmal, A.A., Wang, D., Liu, S., et al. (2012). Targeting FACT complex suppresses mammary tumorigenesis in Her2/neu transgenic mice. Cancer Prev. Res. *5*, 1025–1035. https://doi.org/10.1158/1940-6207.CAPR-11-0529.

31. Garcia, H., Miecznikowski, J.C., Safina, A., Commane, M., Ruusulehto, A., Kilpinen, S., Leach, R.W., Attwood, K., Li, Y., Degan, S., et al. (2013). Facilitates chromatin transcription complex is an "accelerator" of tumor transformation and potential marker and target of aggressive cancers. Cell Rep. *4*, 159–173. https://doi.org/10.1016/j.celrep.2013.06.013.

32. Burkhart, C., Fleyshman, D., Kohrn, R., Commane, M., Garrigan, J., Kurbatov, V., Toshkov, I., Ramachandran, R., Martello, L., and Gurova, K.V. (2014). Curaxin CBL0137 eradicates drug resistant cancer stem cells and potentiates efficacy of gemcitabine in preclinical models of pancreatic cancer. Oncotarget *5*, 11038–11053. https://doi.org/10.18632/oncotarget.2701.

33. Dermawan, J.K.T., Hitomi, M., Silver, D.J., Wu, Q., Sandlesh, P., Sloan, A.E., Purmal, A.A., Gurova, K.V., Rich, J.N., Lathia, J.D., et al. (2016). Pharmacological targeting of the histone chaperone complex FACT preferentially eliminates glioblastoma stem cells and prolongs survival in preclinical models. Cancer Res. *76*, 2432–2442. https://doi.org/10.1158/0008-5472.CAN-15-2162.

34. Fleyshman, D., Prendergast, L., Safina, A., Paszkiewicz, G., Commane, M., Morgan, K., Attwood, K., and Gurova, K. (2017). Level of FACT defines the transcriptional landscape and aggressive phenotype of breast cancer cells. Oncotarget *8*, 20525–20542. https://doi.org/10.18632/oncotarget.15656.

35. Chang, H.W., Nizovtseva, E.V., Razin, S.V., Formosa, T., Gurova, K.V., and Studitsky, V.M. (2019). Histone chaperone FACT and curaxins: effects on genome structure and function. J. Cancer Metastasis Treat. *5*, 78. https://doi.org/10.20517/2394-4722.2019.31.

36. Hsieh, F.K., Kulaeva, O.I., Patel, S.S., Dyer, P.N., Luger, K., Reinberg, D., and Studitsky, V.M. (2013). Histone chaperone FACT action during transcription through chromatin by RNA polymerase II. Proc. Natl. Acad. Sci. USA *110*, 7654–7659. https://doi.org/10.1073/pnas.1222198110.

37. Farnung, L., Vos, S.M., and Cramer, P. (2018). Structure of transcribing RNA polymerase II-nucleosome complex. Nat. Commun. *9*, 5432. https://doi.org/10.1038/s41467-018-07870-y.

38. Kujirai, T., Ehara, H., Fujino, Y., Shirouzu, M., Sekine, S.I., and Kurumizaka, H. (2018). Structural basis of the nucleosome transition during RNA polymerase II passage. Science *362*, 595–598. https://doi.org/10.1126/science.aau9904.

39. Kujirai, T., and Kurumizaka, H. (2020). Transcription through the nucleosome. Curr. Opin. Struct. Biol. *61*, 42–49. https://doi.org/10.1016/j.sbi.2019.10.007.

40. McCullough, L.L., Pham, T.H., Parnell, T.J., Connell, Z., Chandrasekharan, M.B., Stillman, D.J., and Formosa, T. (2019). Establishment and maintenance of chromatin architecture are promoted independently of transcription by the histone chaperone FACT and H3-K56 acetylation in Saccharomyces cerevisiae. Genetics *211*, 877–892. https://doi.org/10.1534/genetics.118.301853.

41. Erkina, T.Y., and Erkine, A. (2015). ASF1 and the SWI/SNF complex interact functionally during nucleosome displacement, while FACT is

required for nucleosome reassembly at yeast heat shock gene promoters during sustained stress. Cell Stress Chaperones *20*, 355–369. https://doi.org/10.1007/s12192-014-0556-x.

42. Singh, R.K., Liang, D., Gajjalaiahvari, U.R., Kabbaj, M.H.M., Paik, J., and Gunjan, A. (2010). Excess histone levels mediate cytotoxicity via multiple mechanisms. Cell Cycle *9*, 4236–4244. https://doi.org/10.4161/cc.9.20.13636.
43. Morillo-Huesca, M., Maya, D., Muñoz-Centeno, M.C., Singh, R.K., Oreal, V., Reddy, G.U., Liang, D., Géli, V., Gunjan, A., and Chávez, S. (2010). FACT prevents the accumulation of free histones evicted from transcribed chromatin and a subsequent cell cycle delay in G1. PLoS Genet. *6*, e1000964. https://doi.org/10.1371/journal.pgen.1000964.
44. Jeronimo, C., and Robert, F. (2016). Histone chaperones FACT and Spt6 prevent histone variants from turning into histone deviants. Bioessays *38*, 420–426. https://doi.org/10.1002/bies.201500122.
45. Odijk, T. (1995). Stiff chains and filaments under tension. Macromolecules *28*, 7016–7018.
46. Bustamante, C., Marko, J.F., Siggia, E.D., and Smith, S. (1994). Entropic elasticity of lambda-phage DNA. Science *265*, 1599–1600.
47. Smith, S.B., Cui, Y., and Bustamante, C. (1996). Overstretching B-DNA: the elastic response of individual double-stranded and single-stranded DNA molecules. Science *271*, 795–799.
48. Chaurasiya, K.R., Paramanathan, T., McCauley, M.J., and Williams, M.C. (2010). Biophysical characterization of DNA binding from single molecule force measurements. Phys. Life Rev. *7*, 299–341.
49. McCauley, M.J., Rueter, E.M., Rouzina, I., Maher, L.J., 3rd, and Williams, M.C. (2013). Single-molecule kinetics reveal microscopic mechanism by which High-Mobility Group B proteins alter DNA flexibility. Nucleic Acids Res. *41*, 167–181. https://doi.org/10.1093/nar/gks1031.
50. Seol, Y., Li, J., Nelson, P.C., Perkins, T.T., and Betterton, M.D. (2007). Elasticity of short DNA molecules: theory and experiment for contour lengths of 0.6–7 μm. Biophys. J. *93*, 4360–4373. https://doi.org/10.1529/biophysj.107.112995.
51. McCauley, M.J., Rouzina, I., Manthei, K.A., Gorelick, R.J., Musier-Forsyth, K., and Williams, M.C. (2015). Targeted binding of nucleocapsid protein transforms the folding landscape of HIV-1 TAR RNA. Proc. Natl. Acad. Sci. USA *112*, 13555–13560. https://doi.org/10.1073/pnas.1510100112.
52. McCauley, M.J., Rouzina, I., and Williams, M.C. (2020). Specific nucleic acid chaperone activity of HIV-1 nucleocapsid protein deduced from hairpin unfolding. Methods Mol. Biol. *2106*, 59–88. https://doi.org/10.1007/978-1-0716-0231-7_4.
53. Jarzynski, C. (1997). Nonequilibrium equality for free energy differences. Phys. Rev. Lett. *78*, 2690–2693.
54. Chen, Z., Gabizon, R., Brown, A.I., Lee, A., Song, A., Díaz-Celis, C., Kaplan, C.D., Koslover, E.F., Yao, T., and Bustamante, C. (2019). High-resolution and high-accuracy topographic and transcriptional maps of the nucleosome barrier. Elife *8*, e48281. https://doi.org/10.7554/eLife.48281.
55. Murugesapillai, D., McCauley, M.J., Huo, R., Nelson Holte, M.H., Stepanyants, A., Maher, L.J., 3rd, Israeloff, N.E., and Williams, M.C. (2014). DNA bridging and looping by HMO1 provides a mechanism for stabilizing nucleosome-free chromatin. Nucleic Acids Res. *42*, 8996–9004. https://doi.org/10.1093/nar/gku635.
56. Jung, Y., and Lippard, S.J. (2003). Nature of full-length HMGB1 binding to cisplatin-modified DNA. Biochemistry *42*, 2664–2671. https://doi.org/10.1021/bi026972w.
57. Heenan, P.R., and Perkins, T.T. (2019). Imaging DNA equilibrated onto mica in liquid using biochemically relevant deposition conditions. ACS Nano *13*, 4220–4229. https://doi.org/10.1021/acsnano.8b09234.
58. Spakman, D., King, G.A., Peterman, E.J.G., and Wuite, G.J.L. (2020). Constructing arrays of nucleosome positioning sequences using Gibson Assembly for single-molecule studies. Sci. Rep. *10*, 9903. https://doi.org/10.1038/s41598-020-66259-4.
59. Brower-Toland, B., and Wang, M.D. (2004). Use of optical trapping techniques to study single-nucleosome dynamics. Methods Enzymol. *376*, 62–72. https://doi.org/10.1016/S0076-6879(03)76005-4.
60. Dodonova, S.O., Zhu, F., Dienemann, C., Taipale, J., and Cramer, P. (2020). Nucleosome-bound SOX2 and SOX11 structures elucidate pioneer factor function. Nature *580*, 669–672. https://doi.org/10.1038/s41586-020-2195-y.
61. Travers, A.A. (2003). Priming the nucleosome: a role for HMGB proteins? EMBO Rep. *4*, 131–136.
62. Anderson, J.D., Lowary, P.T., and Widom, J. (2001). Effects of histone acetylation on the equilibrium accessibility of nucleosomal DNA target sites. J. Mol. Biol. *307*, 977–985. https://doi.org/10.1006/jmbi.2001.4528.
63. Ehara, H., Kujirai, T., Shirouzu, M., Kurumizaka, H., and Sekine, S.I. (2022). Structural basis of nucleosome disassembly and reassembly by RNAPII elongation complex with FACT. Science *377*, eabp9466. https://doi.org/10.1126/science.abp9466.
64. Lowary, P.T., and Widom, J. (1998). New DNA sequence rules for high affinity binding to histone octamer and sequence-directed nucleosome positioning. J. Mol. Biol. *276*, 19–42. https://doi.org/10.1006/jmbi.1997.1494.
65. Muthurajan, U.M., McBryant, S.J., Lu, X., Hansen, J.C., and Luger, K. (2011). The linker region of macroH2A promotes self-association of nucleosomal arrays. J. Biol. Chem. *286*, 23852–23864. https://doi.org/10.1074/jbc.M111.244871.
66. Rogge, R.A., Kalashnikova, A.A., Muthurajan, U.M., Porter-Goff, M.E., Luger, K., and Hansen, J.C. (2013). Assembly of nucleosomal arrays from recombinant core histones and nucleosome positioning DNA. JoVE, 50354. https://doi.org/10.3791/50354.
67. Wenner, J.R., Williams, M.C., Rouzina, I., and Bloomfield, V.A. (2002). Salt dependence of the elasticity and overstretching transition of single DNA molecules. Biophys. J. *82*, 3160–3169.
68. Farge, G., Laurens, N., Broekmans, O.D., van den Wildenberg, S.M.J.L., Dekker, L.C.M., Gaspari, M., Gustafsson, C.M., Peterman, E.J.G., Falkenberg, M., and Wuite, G.J.L. (2012). Protein sliding and DNA denaturation are essential for DNA organization by human mitochondrial transcription factor A. Nat. Commun. *3*, 1013. https://doi.org/10.1038/ncomms2001.

STAR★METHODS

KEY RESOURCES TABLE

REAGENT or RESOURCE	SOURCE	IDENTIFIER
Bacterial and virus strains		
E. coli BL21(DE3) cells for expression	MilliporeSigma	Cat# CMC0014
E. coli Rosetta (DE3)pLysS cells for expression	MilliporeSigma	Cat# 71401
Chemicals, peptides, and recombinant proteins		
Ni^{2+}-NTA resin	Qiagen	Cat# 30250
Glutathione Sepharose	Sigma-Aldrich	Cat# GE17-5131-02
IPTG	RPI	Cat# 32115
LB broth, Miller (Luria-Bertani)	Difco	Cat# 244610
LB agar, Miller (Luria Bertani)	Difco	Cat# 244520
Ampicillin	Gold Biotechnology	Cat# A-301-100
Kanamycin	Teknova	Cat# K2150
Imidazole	Acros	Cat# 122025000
Nickel sulfate	Alfa Aesar	Cat# 12514
PMSF	MP	Cat# 195381
Mini EDTA-free protease inhibitor	Roche	Cat# 791001
BsaI-HFv2 restriction enzyme	NEB	Cat# R3733S
DNA pol I, large (Klenow) fragment	NEB	Cat# M0210L
Digoxygenin-11-dUTP	Sigma	Cat# 11093088910
Biotin-16-dUTP	Sigma	Cat# 11093070910
Biotin-14-dATP	Thermo Fisher	Cat# 19524–016
Biotin-14-dCTP	Thermo Fisher	Cat# 19518–018
HEPES salt	Sigma Aldrich	Cat# H4034
NaOH	Sigma Aldrich	Cat# S8263
NaCl	Sigma Aldrich	Cat# S7653
TRIS pH 7.0 and 8.0	ThermoFIsher	Cat# AM9010
EDTA pH 8.0	ThermoFisher	Cat# AM9010
Critical commercial assays		
Superdex 75 column	Cytiva/GE Healthcare	Cat# 28-9893-33
Superdex 200 column	Cytiva/GE Healthcare	Cat# 28-9893-35
Recombinant DNA		
Plasmid pET28 (modified) cloning vector	Novagen	Cat# 69864
Plasmid pCOLADuet cloning vector	Novagen	Cat# 71406
Plasmid pUC19	Lowary et al.[64]	N/A
601 Widom positioning sequences	McCauley et al.[18]	N/A
Software and algorithms		
LUMICKS python scripts	https://harbor.lumicks.com/	N/A
FIJI	https://fiji.sc/	N/A
Numerical Recipes Algorithms	http://numerical.recipes/	N/A
NI LabWindows CVI	https://ni.com/	N/A
Other		
1.76 μm Streptavidin coated beads	Spherotech	Cat# SVP-15-5
3.11 μm Streptavidin coated beads	Spherotech	Cat# SVP-30-5
2.0–2.4 μm Anti-Dig coated beads	LUMICKS	Cat# 'Buffer Kit'
2.0 μm Protein G coated beads	Spherotech	Cat# PGP-20-5

RESOURCE AVAILABILITY

Lead contact

Further information and requests for resources and reagents should be directed to and will be fulfilled by the lead contact, Mark C. Williams (ma.williams@northeastern.edu).

Materials availability

This study did not generate new, unique reagents.

Data and code availability

All data reported in this paper will be shared by the lead contact upon request. This paper does not report original code. Any additional information required to reanalyze the data reported in this paper is available from the lead contact upon request

METHOD DETAILS

Preparation of DNA constructs

DNA constructs, composed of 12 Widom 601 sequences,[64] flanked by labeled DNA handles, have been described previously.[18] Briefly, a pUC19-based plasmid with an array of 12 nucleosome positioning sequences, each with 147 bp for histone octamer binding and 60 bp linker, was cleaved (*Bsa*I) to create long flanking non-nucleosome positioning handles of 1340 and 1360 base pairs. Restriction endonuclease digestion leaves distinct four-base overhang termini allowing DNA polymerase repair to insert single digoxygenin and biotin tags on opposing termini, for optical tweezers (OT) experiments. These linear 'pJ1937' templates, 5240 bp long, were purified and concentrated to ~1 ng/μL (Figure 1H). A variation on this construct employed longer (3400 bp) handles and single biotin tag on each terminus. This 'pJ2774' template was advantageous for single molecule fluorescence (SMF) imaging and optimal tethering in the laminar flow cell of the LUMICKS SMF apparatus.

Octamer assembly onto DNA

Human histone octamers included either unlabeled histones or histones in which an H2B T112C derivative was labeled with Atto647. Nucleosome reconstitution has been detailed previously.[65,66] Briefly, HPLC-purified octamers, stored in 50% glycerol, were added to positioning sequences in a 1.02 mass ratio of protein:DNA (or ~1.2 octamers for each positioning site). Wild type octamers were reconstituted with the pJ1937 DNA template and tagged octamers with the pJ2774 construct. Reconstitution was achieved in 10 mM Tris-HCl, pH 7.5, 1 mM EDTA, with decreasing stepwise concentrations of NaCl, from 2 M to 2.5 mM over ~30 h. Reconstitutions were determined to be successful when arrays of n > 10 nucleosomes were observed and characterized though AFM imaging (directly counting octamers) and tweezers stretching experiments (counting core disruptions) as controls. Stored at 4 C in 2.5 mM NaCl at a final concentration of ~0.6 μg/μL (~100 nM for both DNA templates), reconstituted arrays remained viable over several weeks.

Preparation/purification of recombinant FACT and FACT domain protein

All the human FACT constructs used in our manuscript were produced in *E. coli* and purified to homogeneity. However, using expression in *E. coli*, we were unable to successfully purify FACT with SPT16 NTD and SSRP1 CTD to homogeneity, as these segments proved to be highly flexible and prone to degradation. SPT16 constructs (501–1006 and 649–926) were cloned in a modified pET28 vector (Novagen) encoding an N-terminal His_6-MBP tag and a tobacco etch virus (TEV) protease cleavage site. SPT16 (927–1006), SSRP1-N1 (1–100) and SSRP1-HMG (551–617) were cloned in a pTEV vector encoding an N-terminal His_6-tag and a TEV protease site. SSRP1-M (196–428) was cloned in a pGST-parallel vector with a TEV protease site. SPT16 (501–644) and SSRP1 (1–617) were cloned in a pCOLADuet vector (Novagen) with no tag. SSRP1-N2 (1–195) was cloned in a pET28a vector encoding an N-terminal His_6-tag and a thrombin cleavage site. The proteins were produced in *E. coli* BL21(DE3) (for SSRP1-N1) or Rosetta (DE3)pLysS (for all other proteins) grown in LB broth at 37°C to an $OD_{600\ nm}$ of approximately 0.6, and then induced with 0.5 mM isopropyl-β-D-thiogalactoside at 15°C for 16 to 20 h. Cells were collected by centrifugation, resuspended in appropriate buffer solutions, and lysed using an Emulsiflex C5 high-pressure homogenizer (Avestin). Proteins were purified by affinity chromatography using Ni^{2+}-NTA resin (Qiagen) or Glutathione Sepharose (Sigma-Aldrich) according to the manufacturers' recommended protocols. The heterodimerization domains of FACT, SPT16 (501–644) and SSRP1-N2 (1–195), were co-expressed and co-purified using Ni^{2+}-NTA resin (Qiagen). To assemble all other SPT16-SSRP1 complexes, the proteins were expressed separately, and the SPT16- and SSRP1-expressing cells were then combined prior to lysis and purification. The His_6, His_6-MBP or GST tags were cleaved by an overnight 4 °C incubation with TEV protease or thrombin. For the His_6-MBP-tagged proteins, the digestion mixture was concurrently dialyzed in 50 mM sodium phosphate, pH 7.5, 300 mM NaCl to remove imidazole, and then applied to a second Ni^{2+}-NTA column to capture the His_6-MBP tag. The SPT16, SPT16-SSRP1 and SSRP1-N1 proteins were further purified by size-exclusion chromatography using preparative Superdex 75 or 200 columns (GE Healthcare) while SSRP1-M was further purified by cation exchange chromatography using a Resource S column (GE Healthcare) in 20 mM MOPS buffer, pH 7.0, developed with increasing NaCl concentration from 40 mM to 1 M.

Dual beam optical tweezers

Dual counterpropagating beam (*Lumics*) optical tweezers were brought to a coincident focus by a pair of confocal objectives (*Nikon*). Within a custom-built fluidic cell, a single streptavidin coated bead (1.76/3.11/5.20 μm diameter, *Spherotech*) was harmonically trapped at the focus of these beams, up to displacement forces of 180 pN. A micropipette (*WPI*) fixed an anti-dig coated bead (2.11 μm diameter, *Spherotech*). A single nucleosome array template involving the pJ1937 construct, suspended between these beads, was stretched by translation (*nPoint*) of the fluidic cell and micropipette tip, with a step size of 4 nm and a pulling rate of ~200 nm/s. Displacement of the trapped bead created deflections in the trapping laser, which were measured on a fast response positioning sensitive detector (*SpotOn*). This deflection was calibrated to a force measurement, by observing the well-known DNA overstretching transition, to provide a dataset of measured forces for set changes in extension. Both the force calibration and a correction in the extension for the finite trap stiffness were characterized for varying bead sizes and solution conditions.[48,67] To characterize the effects of FACT and isolated subunits, proteins were incubated with reconstituted arrays, caught, and then stretched (catching the arrays and then exposing them to proteins led to bead interference due to turbulent flow). Array experiments were concluded after no more than three hours to minimize destabilization observed to occur over time at room temperature.

AFM imaging in liquid

Assembled nucleosome array constructs were diluted to a concentration of ~100 pM in a 10 mM NaCl, 10 mM HEPES, pH 7.5 buffer. For FACT experiments, protein samples were also diluted in the same buffer at set concentrations and incubated with the nucleosomes for 5 min. Samples (20 uL) were deposited on a freshly cleaved mica surface pretreated with a 100 mM $NiCl_2$ solution, rinsed with deionized water and dried, following a protocol developed by the lab of Thomas Perkins.[57] One minute after deposition, the sample was washed with a 50 mM NaCl, 10 mM $NiCl_2$, 10 mM Hepes, pH 7.5 buffer to stabilize DNA attachment to the surface. The sample was imaged in liquid using peak force tapping mode and *Scanasyst-fluid+* 150 kHz silicon nitride probe tips with 2-nm nominal width (*Bruker*). For acquired images, the background was flattened to remove slope and a threshold of 2 nm was applied to identify the locations of histones and a minimum bounding box was calculated for each array. For comparison with simulated arrays (Figure S6), the average apparent diameter of a single histone (which depends on threshold height and tip sharpness) were subtracted from these spread values to determine distances between histone centers. The volumes of single histones were calculated by fitting ellipses to 1-dimensional height profiles of individually resolvable histones and modeling the total volume as a half (flat bottomed) ellipsoid. Effects due to salt solutions that differ from the tweezer experiments are addressed the text and have been characterized previously.[18]

Combined fluorescence and optical tweezers

Fluorescence images (LUMICKS) were collected in the same solution conditions as in the dual beam trap described above. These tethered pJ2774 nucleosome arrays, however, were assembled in parallel channels in a microfluidics cell, as shown in Figure 5B. The pJ2774 construct is the same 12x positioning sequence as the pJ1937 used above, but with longer (~5000 bp) handles and biotin labels on either end, to facilitate both rapid catching and a clearer array image with minimal interference from bead autofluorescence. The pulling rate was set to 200 nm/s, to match the OT experiments above. Imaging was carried out for reconstituted nucleosomes, labeled with Atto647N or Alexa488 at H2B T112C (for two dyes per octamer). Confocal images and kymographs were collected at 40 nm resolution, though these non-STED images are diffraction limited (~400 nm). To minimize fluorophore damage, the power of the excitation laser was minimized to yield the longest measurable decay times in the absence of applied force. Fitted decay lifetimes were further corrected for photobleaching according to Supplement S7.[68] Full FACT and the key domains were incubated with the arrays before tethering, as described above, though the longer tethers also enabled post-tethering exposure to proteins as shown in Figure 5B (for HMGB). No significant difference was seen in the data collected was seen between these two techniques.

QUANTIFICATION AND STATISTICAL ANALYSIS

Modeling dsDNA elasticity

The extensible Worm-like Chain (eWLC) model of polymer elasticity describes the length and flexibility of ds DNA under applied tension.[45–49] As the end-to end extension (b) is increased, the measured force (F) increases as the polymer is first straightened and then elongated. The polymer is characterized by a contour length (B, typically expressed in nm per base pair for a construct of a fixed number of base pairs), the enthalpic stiffness modulus (S, in pN) and a measure of entropically driven DNA curvature termed the persistence length (P, in nm). The high force limit of this expression has a well-known solution:

$$b(F) = B\left[1 - \frac{1}{2}\left(\frac{k_B T}{PF}\right)^{1/2} + \frac{F}{S}\right]. \quad \text{(Equation 1)}$$

A cycle of extension and release for the DNA template is shown in Figure S1A, fitted extension data is shown in Figure S1B. Fitting returned $B = 0.340 \pm 0.001$ nm/bp, $S = 1000 \pm 100$ pN and $p = 42 \pm 1$ nm averaged over $N = 5$ (errors are SEM). These are typical values and include known variations in fitted parameters for relatively shorter construct lengths.[18,50] The eWLC model and these parameters are used to convert between the *force-dependent* length of dsDNA and the *force-independent* number of bases measured freed from

the nucleosome in Figures 2 and 3 and Table S2. Furthermore, at each stage of the extension cycle, the force dependent extension of DNA ($b(F)$) is simply the length not wrapped around an octamer. The extension is determined by Equation 1, where B is the length of the handles and the linkers plus the length of any DNA released disrupted nucleosome (see Figure 2B). While a fully disrupted nucleosome may remain attached to the DNA at the central dyad, this binding does not appear to affect dsDNA elasticity in a measurable way for these experiments.

In contrast, and as we have shown in previous work, protein binding to DNA induces a measurable change in the fitted persistence length.[18,49] An example of a fit to dsDNA in 125 FACT is shown in Figure S1C. Variations in the fitted value of the persistence length for added protein are analyzed below.

Identifying DNA release from the force extension data

The release of DNA from the strong site is characterized by a measured increase in length at each release event. As discussed in the text, the outer ½ wraps release below 10 pN, while the inner wraps held closely to the histone core ('strong') sites release above 10 pN (as in Figure 2B).

Within an array, the outer ½ turn releases are in equilibrium, and are generally not distinguishable in these experiments. Thus, the change in extension is measured between 2 and 5 pN (x_{outer}), corrected for the elasticity of dsDNA and then converted to base pairs using Equation 1. Release of the outer wrap was characterized where possible when complete low extension data could be observed.

Individual releases of DNA from the inner wrap may be identified by a discrete 'rip' in the force extension data. The finite stiffness led to a definite drop in the measured force as well as an extension increase. This was exploited to create thresholds in force (typically 0.3 pN) and extension (typically 8 nm). This effectively eliminated false detections due to instrument noise or protein-DNA aggregation During force-extension of an array, high force 'rips' were counted above a threshold of 10 pN. Native arrays with less than 11 'rips' were discounted, due to concerns of incomplete array reconstitution or possible loss of nucleosomes from destructive forces that arise during tethering. When incubated with protein, arrays of 9 events or greater were retained, though some data on a 12x array was collected at each concentration to minimize bias due to any missing octamers (this was most difficult for SPT16 domains that aggregated DNA at very high concentrations). Furthermore, protein aggregation did often lead to large DNA-induced looping that was easily identified, as aggregate/loop release leads to much larger events (>100 nm, typically) that may be disregarded. Finally, these measurements were processed as described in Figure 2 (analyzing force dependent polymer lengths is also discussed in Figure S1, while distributions of released length and forces at each A appear in Figure S2).

Determining forces and the kinetics of strong site disruption

The release of DNA from the strong sites for each of the $N = 30$ arrays is plotted in the sequence of release in Figure S2A and averaged values are shown in Figure S2B. A combination of applied tension and random thermal fluctuations drive the non-equilibrium release of DNA from the inner wrap. Force facilitates this release, favoring the unwrapped state and increasing the probability of observing release. This probability will decrease as the number of nucleosomes remaining on the array decreases. For a given number of nucleosomes remaining on the array (A), the average release force will vary as shown previously[18];

$$F_{avg} = \frac{k_B T}{x^{\dagger}_{core}} \cdot \ln\left[\frac{dF}{dt} \cdot \frac{x^{\dagger}_{core}}{k_B T \cdot k_0 \cdot A}\right]. \quad \text{(Equation 2)}$$

The loading rate (dF/dt) in these experiments is fixed at 7 pN/s, while both the distance to the transition state ($x^{\dagger}_{core}$) and the zero-force opening rate (k_o) are fitting parameters to the data. Importantly, the breathing rate is not a rate of complete, simultaneous outer and inner wrap release, but the fluctuational zero force rate of opening for the last (out of several) strongest transition barrier for the strong sites unwrapping. A fit to the data is shown in Figures S2B and 2E. As the process of catching the nucleosomes may least to some disruption that could affect the results, it is useful to compare the fit to all 12x releases to the highest (last) 10x nucleosomes. Here, the results to not differ within uncertainty. Finally, a distribution of all opening events in Figure S2C allows a comparison of the fitted parameters from fits to Equation 2, where the uncertainty in the fits to the zero-force opening rate is used in a Monte-Carlo simulation. The non-Gaussian nature of both the data and the model are evident. Fitted parameters for nucleosomes and protein saturated nucleosomes are summarized in Table S2.

Measuring DNA lengths released from nucleosome strong sites of the core

The release of DNA from the strong site is characterized by a measured increase in length at each release event. This length is measured for each nucleosome in the array (A is the number remaining, Figure S2D) and is converted to a force independent value in base pairs in Figure S2E. The average value appears to be the same across the array within experimental error. An average value of DNA held to the strong sites is determined to be $x_{core} = 71.8 \pm 0.4$ base pairs (SEM), and this result is shown in Figure 2F (Figure S2F) and Table S2. This process was repeated across experiments in the presence of FACT and several domains. These results are summarized in Table S1 and Figure 3F.

Quantifying protein-nucleosome binding through variations in the force driving inner wrap release

Averaging the observed force required to release the inner wrap across all A gives $F_{nucl} = 24.3 \pm 0.2$ pN. This value is observed to vary with increasing concentrations of protein (Figure 3B), which bind to nucleosomes and either weaken or stabilize histone DNA binding up to a concentration that corresponds to protein saturation ($F_{protein}$), according to a simple model[18,49]:

$$F(\Theta) = F_{nucl} - (F_{nucl} - F_{protein}) \cdot \Theta \cdot \quad \text{(Equation 3)}$$

Here the occupancy (Θ), varies from zero to unity according to the well-known Hill Eq.:

$$\Theta = \frac{1}{1 + \left(\frac{K_D}{c}\right)^H} \cdot \quad \text{(Equation 4)}$$

Increasing concentrations (c) effect the occupancy through the equilibrium dissociation constant (K_D), and a cooperativity parameter (H, here set to unity). Thus, non-linear fits determined values for K_D and $F_{protein}$, and these are shown for FACT and the key active domains SSRP1 HMGB and SPT16 MD in Table S1 and in Figure 3C.

Quantifying protein-DNA binding through variations in the dsDNA persistence length

Constructs with no nucleosomes present were also force extended, to determine dsDNA flexibility in the absence and presence of protein. These curves were fit to the eWLC as discussed above and shown in Figure S1. Repeating these measurements and analysis for varying concentrations of protein will show variations in eth fitted persistence length[18,49]:

$$\frac{1}{P(\Theta)} = \frac{1 - \Theta}{P_{DNA}} + \frac{\Theta}{P_{protein}} \cdot \quad \text{(Equation 5)}$$

Again, the occupancy is coupled to the Hill Eq. above. It was not practical to deduce all free parameters from each fit, so the value of P_{DNA} was fixed at 42 nm and $P_{protein}$ at 8 nm ($H = 1$ as well). Fitted values of K_D are shown in Table S1 and graphically in Figure 3C.

Calculating the energy of histone-DNA disruption

Figure S4A illustrates a typical cycle of extension and release, including polymer models of Equation 1 used to characterize the length of the construct with varying numbers of intact nucleosomes present. As detailed in Figure 2, at low forces, the outer ½ wraps of DNA release from the histone tails. These 12x disruptions are indistinguishable. Direct integration between extension and release, as shown in Figure S4B, gives an average work done for each unwrapping event of 15 k_BT. As this is an equilibrium process, this work corresponds directly to the free energy of the release of the outer wrap from the histone tails. Notably, in the presence of saturating concentrations of FACT, this energy decreases to zero, as extension and release are both indistinguishable from the elastic response of dsDNA.

The non-equilibrium release of DNA from the inner wrap may be determined for each disruption as in Figure S4C. The work done for each release (W_A) is the difference in energy for the array before (ΔG_A) and after release (ΔG_{A-1}) and including a correction for the stiffness of the instrument $W_{stiffness}$. Array energies are determined by numerical integration of the eWLC model of Equation 1, up to the measured opening force (F) and including the opening length of the inner wrap (x_{core})[51,52];

$$W_A = \Delta G_A - \Delta G_{A-1} + W_{stiffness} \cdot \quad \text{(Equation 6)}$$

To convert this work to the equilibrium energy of release requires the method of Jarzynski[53]:

$$\Delta G_{core} = -k_B T \cdot \ln\left[\sum e^{-W/k_B T}\right] \cdot \quad \text{(Equation 7)}$$

All numbers are summarized with uncertainties in Table S2 and graphically in Figures 2G and 3J.

Measuring the energy barrier of inner wrap disruption

Kinetic fits to Equation 2 facilitate a closer examination of the transition state barrier. The distribution of release forces provides details on the transition state. For a given loading rate ($r = 10$ pN/s) and barrier shape (ν is chosen to be ½) the probability of observing the maximum force in the distribution (P_{max} at F_{max}) characterize the transition state. Here, with the transition state parameters of the opening rate (k_o) and the distance to the barrier ($x^{\dagger}_{core}$) already known, we use a simplified expression to determine the barrier height ($G^{\dagger}_{core}$)[51,52];

$$G^{\dagger}_{core} = \frac{F_{\max} \cdot x^{\dagger}_{core}}{k_B T}\left[\frac{x^{\dagger}_{core}}{x^{\dagger}_{core} - P_{\max} \cdot k_B T \cdot e}(1 - \nu)\right] \cdot \quad \text{(Equation 8)}$$

For each released nucleosome within the array (A), the distribution of the inner wrap release is smoothed, and fit to a gaussian. Fitted values of the mean and the standard deviation allow direct determination of P_{max} at F_{max} at each value of A (see Figure S4). The value of the distance to the transition state, determined from fits to Equation 2, was varied to minimize the variability between low and high values of A, which arose from noise in the fits. Here $x^{\dagger} \sim 0.75$ nm was the final value used similar to the distance to the transition state fitted from the dependence of the average release force vs the number of nucleosomes left in the array

(Figure S2B). Calculated values of the barrier height are averaged over all values of A, giving $G^{\dagger}_{core} = 22 \pm 7\ k_BT$ for the nucleosome inner wrap in the absence of FACT, and $G^{\dagger}_{core} = 6 \pm 1\ k_BT$ in saturating concentrations of full FACT. Errors are SEM from the values averaged over all values of A. Varying either $x^{\dagger}_{core}$ or ν (which specifically may take the values of 1/2 or 2/3) changes these final values somewhat, but not the relative decrease as a saturating concentration of FACT was added to nucleosomes. FACT induces a significant drop in the barrier height to DNA-histone disruption of the strong sites.

AFM image analysis

Images reveal the location and organization of nucleosomes and DNA handles. However, it is not always possible to uniquely trace the DNA backbone through the array. In previous work, these locations were analyzed to deduce the lengths of DNA unwound from the nucleosome.[18] Here, as full FACT is added, nucleosomes are remodeled, and become difficult to distinguish among crossing strands of DNA and non-bound proteins. An approach that gives a consistent analysis for these conditions measures a height across the array image, as shown in Figures S5A and S5B, which distinguishes histones from protein free DNA. The smallest rectangle that encloses all histones (regions above a 2 nm threshold) is defined as the 'spread', as in Figure S5C. This spread is directly related to the length of linker DNA; as DNA unwinds from the nucleosome, the spread increases. Simulations of arrays deposited on the surface quantify this relationship, in Figures S5D and S5E. The direction of the DNA linkers between the histones are simulated assuming they follow a 3D worm like chain with persistence length 45 nm and length determined by the amount of DNA released.

Confocal/Kymograph image analysis

Images were processed with custom Python scripts based upon those available from LUMICKS, using available Pylake functions. To quantify the kinetics of histone release, the intensity for a row of pixels was graphed over time using the Fiji/ImageJ application. Fiji/ImageJ was also used to fit the decay to a single exponential, allowing the extraction of a fitted rate of decay. A minimum of 3 arrays was characterized for each condition shown in Figure 5G.

Correction to measured lifetimes due to photobleaching

Though the rate of photobleaching is slow compared to the fluorescence decays measured in Figures 5E and 5F, photobleaching was experimentally characterized. A tethered array was held at 1 pN, in the absence of any chaperone protein. Confocal laser power and all other experimental parameters were fixed as with other experiments. Fitting these measured decays to a single exponential gives a photobleaching rate of $k_p = 12 \pm 3\ ms^{-1}$. This is used to correct the measured rates of nucleosome release (alone and in the presence of FACT and its subunits) according to the simple expression[68]:

$$I = I_o \cdot e^{-t_{release} \cdot k_{release}} \cdot e^{-t_{bleach} \cdot k_{bleach}}. \quad \text{(Equation 9)}$$

In these experiments, t_{bleach} and $t_{release}$ are the same, as the arrays are tethered and imaged in the same flow channel. Even in experiments where the arrays were translated to a new channel, these times should be very nearly identical (differences of only a few seconds), since release was constrained by holding the tension to only 1 pN, inhibiting release, until higher tension was applied. Any error in this assumption should be much less than the error in the combined and propagated results.